Title

Arrestin-dependent nuclear export of phosphodiesterase 4D promotes GPCR-induced nuclear cAMP signaling required for learning and memory



Journal

Science Signaling, 16(778)

ISSN

1945-0877

Authors

Martinez, Joseph M

Shen, Ao

Xu, Bing

et al.

Publication Date

2023-03-28

DOI

10.1126/scisignal.ade3380

Peer reviewed

HHS Public Access

Author manuscript

*Sci Signal*. Author manuscript; available in PMC 2023 August 05.

Published in final edited form as:

*Sci Signal*. 2023 March 28; 16(778): eade3380. doi:10.1126/scisignal.ade3380.

# Arrestin-dependent nuclear export of phosphodiesterase 4D promotes GPCR-induced nuclear cAMP signaling required for learning and memory

**Joseph M. Martinez**[1], **Ao Shen**[1,2], **Bing Xu**[1,3], **Aleksandra Jovanovic**[1], **Josephine de Chabot**[1], **Jin Zhang**[4], **Yang K. Xiang**[1,3,*]

[1]Department of Pharmacology, University of California at Davis, Davis, CA, 95616, USA

[2]School of Pharmaceutical Sciences and the Fifth Affiliated Hospital, Guangzhou Medical University, Guangzhou, 511436, China

[3]VA Northern California Health Care System, Mather, CA, 95655, USA

[4]Department of Pharmacology, University of California at San Diego, San Diego, CA, 92093, USA

## Abstract

GPCRs promote the expression of immediate early genes required for learning and memory. Here, we showed that $\beta_2$-adrenergic receptor ($\beta_2$AR) stimulation induced the nuclear export of phosphodiesterase 4D5 (PDE4D5), an enzyme that degrades the second messenger cAMP, to enable memory consolidation. We demonstrated that the endocytosis of $\beta_2$AR phosphorylated by GPCR kinases (GRKs) mediated arrestin3-dependent nuclear export of PDE4D5, which was critical for promoting nuclear cAMP signaling and gene expression in hippocampal neurons for memory consolidation. Inhibition of the arrestin3-PDE4D5 association prevented $\beta_2$AR-induced nuclear cAMP signaling without affecting receptor endocytosis. Direct PDE4 inhibition rescued $\beta_2$AR-induced nuclear cAMP signaling and ameliorated memory deficits in mice expressing a form of the $\beta_2$AR that could not be phosphorylated by GRKs. These data reveal how $\beta_2$AR phosphorylated by endosomal GRK promotes the nuclear export of PDE4D5, leading to nuclear cAMP signaling, changes in gene expression, and memory consolidation. This study also highlights the translocation of PDEs as a mechanism to promote cAMP signaling in specific subcellular locations downstream of GPCR activation.

[*]Corresponding Author: Yang K. Xiang, Department of Pharmacology, University of California at Davis, CA 95616, USA, ykxiang@ucdavis.edu.

**Author Contributions:** Conceptualization: JMM, AS, YKX. Methodology: JMM, AS, YKX. Investigation: JMM, AS, AJ, BX, JDC. Visualization: JMM, YKX. Funding acquisition: YKX, JMM. Project administration: YKX, JMM, AS. Supervision: YKX. Writing – original draft: JMM, YKX. Writing – Review and editing: JMM, AS, JZ, YKX. JMM and AS contributed to the study equally.

**Competing Interest Statement:** No competing interests to declare.

Supplementary Materials:

Fig S1–S9.

Table S1.

## Introduction

Cyclic adenosine monophosphate (cAMP) is an essential secondary messenger for neurohormonal actions in mammalian cells (1). Spatiotemporal regulation of cAMP signals targets specific substrates during different cellular responses. For example, when GPCRs are activated, they can increase ion channel activity at the plasma membrane (PM) and increase nuclear cAMP signaling to promote gene expression for tissue remodeling and adaptation. The $\beta_2$AR is important for hippocampal learning and memory and can transduce nuclear cAMP signals (2–6). In hippocampal neurons, nuclear cAMP can promote cAMP-response element-binding protein (CREB)-dependent immediate early gene (IEG) expression (7), which is considered the molecular basis of hippocampal long-term potentiation, learning, and memory consolidation (8, 9). However, the mechanism by which receptor stimulation leads to cAMP signaling in different cellular compartments, such as the nucleus, remains unclear.

Agonist stimulation of the $\beta_2$AR promotes phosphorylation of the receptor at different sites by G-protein receptor kinase (GRK) and protein kinase A (PKA) (10), creating two distinct subpopulations with different signaling pathways (11–13). The GRK-phosphorylated subpopulation of $\beta_2$ARs is essential for receptor endocytosis in fibroblasts and hippocampal neurons (14, 15). Additionally, the endocytosis of $\beta_2$AR is necessary for agonist-induced expression of genes (16–21). On the other hand, phosphodiesterases (PDEs) are a family of enzymes that play a crucial role in refining the spatiotemporal dynamics of local cAMP signaling by hydrolyzing cyclic nucleotides at different subcellular organelles and structures. Phosphodiesterase 4D (PDE4D) isoforms are closely linked to $\beta_2$AR functionally and physically and are essential for the subcellular cAMP signaling induced by $\beta_2$AR (22–26). When $\beta_2$AR is stimulated, arrestins can recruit PDE4D to the receptor (26). However, the recruitment of arrestin to the receptor is abolished if the GRK phosphorylation sites of $\beta_2$AR are mutated (15). Moreover, inhibiting GRK2 prevents PDE4D interaction with $\beta_2$AR (27). The dynamic association of PDE4D with the activated $\beta_2$AR may cause PDE4D to redistribute inside a cell, which, in turn, creates cAMP microdomains and gradients of cAMP (24, 28–32). This may facilitate the propagation of cAMP signals into the nucleus to promote gene expression.

In this study, we identified the PDE4D family member PDE4D5 as being enriched in the nucleus of cortical and hippocampal neurons. We demonstrated that stimulation of GPCRs, such as that of $\beta_2$AR, could lead to the trafficking of PDE4D5 out of the nucleus. This process was inhibited in neurons expressing GRKΔ-$\beta_2$AR, a mutant receptor that could not be phosphorylated by GRK, which impaired nuclear cAMP signaling, IEG expression, and memory consolidation in mice. However, inhibition of PDE4 rescued nuclear signaling in GRKΔ neurons, thereby ameliorating the memory deficiency in mice expressing GRKΔ-$\beta_2$AR. Our findings suggest a potential mechanism in which GRK-phosphorylated $\beta_2$AR sequesters nuclear PDE4D5, indirectly promoting nuclear cAMP signaling and gene expression.

## Results

### A subpopulation of GRK-phosphorylated $\beta_2$AR promotes agonist-induced nuclear cAMP signaling and immediate early gene expression.

Stimulation with the β-agonist isoproterenol (ISO) promoted GRK phosphorylation of both $Ser^{355}$ and $Ser^{356}$ in a subpopulation of $\beta_2$AR, which underwent endocytosis and displayed an intracellular distribution in primary hippocampal neurons (Figure 1A), consistent with our previous report (14). Another subpopulation of $\beta_2$AR phosphorylated by PKA at both $Ser^{261}$ and $Ser^{262}$ remained at the plasma membrane (PM). We sought to explore the functional consequences of differentially phosphorylated $\beta_2$AR subpopulations by examining subcellular cAMP dynamics assessed with the FRET-based cAMP biosensor ICUE3 targeted to the plasma membrane (PM-ICUE3) or the nucleus (NLS-ICUE3) (Figure 1B). First, we determined the effects of pharmacological inhibition of GRKs or PKA on subcellular cAMP dynamics. Neurons from $\beta_1/\beta_2$AR double knockout (DKO) mice were co-transfected with cAMP ICUE3 biosensors and wild-type (WT) $\beta_2$ARs to isolate receptor action. Inhibition of GRKs with paroxetine, but not inhibition of PKA with H89, attenuated nuclear cAMP signaling but leaving the cAMP signal at the PM intact (Figure 1C – 1G). Inhibition of GRKs also attenuated the expression of IEGs such as *cFOS*, *FOSB*, *RHOB*, and *OLIG2* (figure S1A – S1D). Paroxetine is also a selective serotonin reuptake inhibitor (SSRI). Fluoxetine, a structurally similar SSRI that does not inhibit GRKs, did not affect the ISO-induced cAMP signal or IEG expression (Figure 1D – 1G and figures S1A – S1D).

To independently verify these observations, neurons from $\beta_1/\beta_2$AR DKO mice were transfected with WT-$\beta_2$AR or mutant $\beta_2$AR with point mutations at both GRK phosphorylation sites (S355/356A) or both PKA phosphorylation sites (S261/262A). Utilizing a $\beta_2$AR active conformation-specific and $G\alpha_s$ mimetic nanobody 80 (Nb80) (33), we showed similar increases in the binding of WT and mutant $\beta_2$ARs after stimulation with ISO (figure S1E and S1F). Thus, these point mutations did not prevent $\beta_2$AR from achieving an active conformational state and engaging G protein binding to promote cAMP generation. $\beta_2$AR stimulation generated equivalent cAMP signals at the PM in DKO neurons expressing WT, GRKΔ, or PKAΔ $\beta_2$AR (Figure 1H – 1J). Deletion of the GRK but not of the PKA phosphorylation sites attenuated $\beta_2$AR stimulation-induced nuclear cAMP signal (Figure 1H, 1K, and 1L). In agreement, deletion of the GRK but not PKA phosphorylation sites of $\beta_2$AR reduced $\beta_2$AR stimulation-mediated expression of IEGs, suggesting that phosphorylation of $\beta_2$AR by GRK was necessary to promote nuclear cAMP signaling and subsequent gene expression (figure S1G – S1J). Additionally, pretreatment of WT $\beta_2$AR-expressing neurons with the endocytosis inhibitor Dyngo4A attenuated cAMP signal in the nucleus but not at the PM (figure S1K and S1L). Moreover, IEG expression in hippocampal neurons was inhibited by nuclear but not cytosolic expression of the protein PKA inhibitor PKI (Figure S1M and S1N). Together, these data indicate that the $\beta_2$AR-mediated nuclear cAMP signal requires GRK-mediated phosphorylation at $Ser^{355/356}$ in $\beta_2$AR and receptor endocytosis and that the nuclear cAMP signal affects IEG expression by activating nuclear PKA.

## GRK-mediated phosphorylation of $\beta_2$AR is necessary for agonist-induced nuclear export of PDE4D5.

Intracellular cAMP microdomains are established in part by various isoforms of phosphodiesterase (PDE), including PDE4D isoforms associated with $\beta_2$AR (24–26, 30), to prevent the nonspecific activation of downstream substrates. We tested whether GRK-phosphorylated $\beta_2$ARs mobilized the distribution of PDE4D isoforms to facilitate the nuclear cAMP signal. In WT primary hippocampal neurons, PDE4D5 was enriched in the nucleus, whereas PDE4D8 and PDE4D9 were mainly distributed in the cytoplasm. (Figure 2A and 2B). In contrast, PDE4B also displayed a cytoplasmic distribution, consistent with a previous report showing a function of PDE4B at the PM (22) (Figure 2A). The specificity of the PDE4D5 antibody was validated using PDE4D knockout and WT MEFs (figure S2A).

We then focused on the effects of $\beta_2$AR stimulation on the distribution of PDE4D5. We found that stimulation with ISO caused the nuclear export of PDE4D5 into the cytoplasm in WT hippocampal neurons (Figure 2C – 2E). We also examined neurons from GRKΔ knock-in mice, which endogenously express the $\beta_2$AR with an S355/356A mutation (figure S2B). The hippocampi from GRKΔ and WT mice had similar morphology, total abundance of $\beta_2$AR and PDE4, and cAMP levels (figure S2C – S2H). There was differential expression of specific PDE4 isoforms in WT compared to GRKΔ hippocampi (figure S2I and S2J). We observed that PDE4D5 was enriched in the nucleus in GRKΔ hippocampal neurons and remained in this subcellular compartment after stimulation with ISO (Figure 2C – 2E). Moreover, the nuclear export of PDE4D5 was independently confirmed with immunoblotting of nuclear fractions from mouse brain slices lysed after clenbuterol-induced $\beta_2$AR stimulation. WT but not GRKΔ slices showed a decrease in PDE4D5 in the nuclear fraction after clenbuterol stimulation (figure S3A). These data indicate that the phosphorylation of $\beta_2$AR at the GRK site is necessary for PDE4D5 trafficking out of the nucleus.

We further assessed whether PDE4D5 trafficking was induced by the stimulation of other GPCR in WT neurons. Although stimulation with ISO promoted robust nuclear export of PDE4D5, other $G\alpha_s$-PCR agonists such as dopamine, cGRP, and urocortin did not elicit complete movement of PDE4D out of the nucleus but caused a change in PDE4D5 distribution around the nuclear envelope (figure S3B and S3C). In comparison, some $G\alpha_q$-PCR agonists did not elicit the nuclear export of PDE4D5 (figure S3C). Moreover, whereas stimulation with ISO caused robust increases in IEG expression, dopamine elicited only small increases in IEG expression, and cGRP and PGE1 did not affect IEG expression (figure S3D).

## The nuclear export of PDE4 plays a critical role in $\beta_2$AR endocytosis-dependent nuclear cAMP signaling.

Arrestins bind to GRK-phosphorylated $\beta_2$AR (34) and recruit PDE4D to activated receptors to attenuate cAMP signaling. We utilized a membrane-permeant peptide derived from arrestin-3, Pep-arr3, to inhibit arrestin-PDE4 binding. Pep-arr3, but not a mutant control peptide with multiple charged amino acids replaced by alanine, prevented agonist-induced PDE4D5 association with activated $\beta_2$AR (Figure 3A and 3B). Pep-arr3 but not the control

peptide, also blocked ISO-induced nuclear export of PDE4D5 in WT hippocampal neurons (Figure 3C and 3D). Consequently, Pep-arr3 but not the control peptide, attenuated $\beta_2$AR-mediated nuclear cAMP signaling in WT neurons (Figure 3E – 3G). Pep-arr3 did not prevent endocytosis of $\beta_2$AR induced by ISO stimulation (figure S4A). We also utilized barbadin, an arrestin3-AP2 interaction inhibitor, which allows the formation of the arrestin-GRK-$\beta_2$AR complex but prevents arrestin and clathrin-dependent receptor endocytosis (35). Barbadin prevented the endocytosis of $\beta_2$AR, nuclear export of PDE4D5, and nuclear cAMP production upon $\beta_2$AR stimulation (figure S4A and Figure 3H and 3I). Further, the application of various endocytosis inhibitors blocked nuclear cAMP signals induced by $\beta_2$AR in WT neurons (Figure 3J and 3K, figure S4B and S4C). Together, these data support that GRK phosphorylation and receptor endocytosis are necessary for $\beta_2$AR-induced and arrestin-mediated nuclear export of PDE4D5, which is critical for cAMP signal propagation to the nucleus.

## Loss of the GRK phosphorylation sites in $\beta_2$AR causes deficits in gene expression and memory retention in a Morris water maze paradigm.

We further assessed the functional consequences of the loss of GRK phosphorylation of $\beta_2$AR (GRKΔ mice) in spatial learning and memory using a Morris water maze paradigm (Figure 4A and figure S5A). WT and GRKΔ mice learned the maze task with similar path efficiency to the platform (Figure 4B). Although GRKΔ mice swam slower than WT mice (figure S5B), WT and GRKΔ mice swam similar distances to the escape platform as indicated by the corrected integrated path length (CIPL, Figure 4C and 4D). These metrics, which are independent of swim speed, indicated that WT and GRKΔ mice learned the maze task despite the differences in latency (time) to escape the platform between groups (figure S5C). There were no differences during maze training in thigmotaxic behavior between mice groups indicating similar stress/anxiety responses during training (Figure 4E). In the probe trial at 24hr after the last training trial, GRKΔ mice spent less time in the target quadrant with the previous escape platforms than WT mice (Figure 4F and figure S5D, S5I, and S5J). WT mice also found the location of the escape platform more quickly and had a shorter CIPL than GRKΔ mice, whereas GRKΔ mice spent more time in the start quadrant (Figure 4G and figure S5D, S5E, S5I, and S5J). There were no differences in the times spent in the thigmotaxic zone, swim speeds, or path efficiencies during the probe trial (figure S5F – S5H). These data suggest that GRKΔ mice have a deficit in remembering the location of the escape platform during the probe trial.

Binned heat maps of probe trial performance indicated that WT mice displayed quick and precise movement to the target quadrant and perseverated near the vicinity of the target (figure S5I and S5J). Conversely, GRKΔ mice were slow to reach the target quadrant and spent relatively little time in the target area (Figure 4G). GRKΔ mice also showed greater initial heading error than WT mice (figure S5K). These data indicate GRKΔ mice have poorer memory of the platform location. We also used a working-memory variant of the Morris water maze (WM-MWM), in which the platform location and start location change daily (figure S6A). Thus, the WM-MWM teaches mice to find the platform day to day, but the memory of the previous platform location does not help performance. Over the six days of training, GRKΔ and WT mice had similar trial-to-trial performances in the WM-MWM

(Figure 4H and 4I, and figure S6B – S6E). Together, these data suggest that GRKΔ mice have intact working memory but impaired long-term memory retention.

We next examined IEG expression because IEG expression may be impaired in GRKΔ mice lacking endocytosis following $\beta_2$AR stimulation (16). WT and GRKΔ hippocampi were harvested 1-hour after MWM training ended on day 5 (Figure 5A and figure S7A – S7F). MWM training increased *cFOS* and *FOSB* expression in WT mice but not in GRKΔ mice (Figure 5B and 5C). *RHOB* and *OLIG2* expression was not changed with MWM training (figure S7G and S7H). In comparison, in response to acute stress induced by a forced swim test (FST), both GRKΔ and WT mice showed increased *cFOS* and *FOSB* expression (Figure 5D – 5F) and no differences in acute anxiety responses (Figure 5G), suggesting acute stress-mediated transcriptional regulation of IEGs was not affected by GRK phosphorylation of $\beta_2$AR. We also assessed the general activity and anxiety responses of GRKΔ and WT mice in an elevated plus maze (EPM) and an open field activity assay. The EPM takes advantage of instinctual predation avoidance behaviors in mice. GRKΔ mice spent more time in the open arms of the EPM than WT mice (figure S8A) but did not show differences in activity in the EPM (figure S8B and S8C). WT and GRKΔ mice showed no differences in general activity in the open field test (figure S8D and S8E). Together, these data indicate no differences between WT and GRKΔ mice in the general activity and acute response to stress but an inverse anxiety response in GRKΔ mice relative to WT controls.

We further examined subcellular cAMP dynamics in WT and GRKΔ neurons. We observed a loss of nuclear cAMP signal in GRKΔ neurons preincubated with the $\beta_1$AR inhibitor CGP20712a (CGP) before $\beta_2$AR stimulation with ISO (Figure 5H – 5K). CGP did not affect ISO-induced cAMP signal on the PM in WT and GRKΔ neurons (Figure 5L – 5O). In contrast, selective activation of $\beta_1$AR with ISO in the presence of the $\beta_2$AR inhibitor ICI118551 induced similar cAMP levels between WT and GRKΔ neurons (figure S8F – S8I). In the absence of inhibitors, GRKΔ and WT neurons showed similar PM and nuclear cAMP signaling in response to βAR stimulation (Figure 5H – 5O). Together, these data suggest that GRK-mediated phosphorylation of $\beta_2$AR is necessary for nuclear cAMP signaling and that loss of this phosphorylation impairs nuclear cAMP signaling and learning-mediated IEG expression, leading to memory consolidation deficits.

## PDE4 inhibition rescues behavioral performance in mice expressing $\beta_2$AR lacking the GRK phosphorylation sites.

We further tested whether inhibition of PDE4 could rescue nuclear cAMP signaling in GRKΔ mice lacking the GRK-phosphorylated $\beta_2$AR subpopulation. We found that inhibition of PDE4 but not of PDE3 rescued nuclear cAMP signaling in GRKΔ hippocampal neurons and modestly increased nuclear cAMP signaling in WT neurons (Figure 6A – 6C and figure S9A and S9B). We then examined if inhibition of PDE4 rescued memory retention in the MWM in GRKΔ mice. GRKΔ mice were given the PDE4 inhibitor roflumilast or vehicle control 1 hour before or 3 hours after MWM testing (figure S9C). All groups were able to learn the maze task (Figure 6D – 6I), although there were differences in swim speed between groups during maze learning. All groups had similar probe trial escape latencies, path efficiency, CIPL, thigmotaxis, and swim speeds (Figure 6J and figure S9D –

S9G). However, the roflumilast pretreatment group spent more time in the target quadrant than the other two groups in the probe trial (Figure 6K and figure S9H). Binned heatmaps from the probe trial suggested that the roflumilast pretreatment group rapidly approached the target quadrant and spent more time near the target than vehicle-treated mice (figure S9H). In comparison, mice treated with roflumilast after MWM training followed a pattern similar to the vehicle group with a similar initial heading error during the probe trial (figure 9I). These data suggest a partial rescue of memory retention with roflumilast pretreatment and highlight the essential role of PDE4D5 nuclear export in promoting nuclear cAMP signal and learning and memory (Figure 6L).

## Discussion

Activation of $G\alpha_{s/olf}$-coupled GPCRs induces cAMP at different subcellular locations to promote distinct cellular actions. In the nucleus, cAMP activates PKA- and CREB-dependent transcription of IEGs such as *cFOS* and *FOSB* to promote long-term potentiation and long-term memory formation (8, 9). The mechanism by which GPCR-induced cAMP signaling remains localized at the PM versus the nucleus remains incompletely understood. Endosomal GPCRs are postulated to deliver cAMP to the nucleus, promoting gene expression in physiology and disease (36). Conversely, PDEs have a critical role in regulating subcellular GPCR signaling by preventing the free diffusion of cAMP through hydrolysis (24, 28–32). Our data provide further evidence to support a potential mechanism in which endosomal $\beta_2$AR-dependent export of the nuclear-localized PDE4D5 is a critical step in promoting the accumulation of the nuclear cAMP signal and IEG expression in memory and learning processes. This mechanism is integral to the regulation of GPCR-induced nuclear signaling and consequently the formation of memory and learning.

Agonist stimulation promotes the trafficking of a subpopulation of GRK-phosphorylated $\beta_2$AR to endosomes in hippocampal neurons (14). The endocytosis of this $\beta_2$AR subpopulation is mediated by arrestin3 binding to $\beta_2$AR, which is blocked when the GRK phosphorylation sites of the receptor are mutated (15). In the resting state, $\beta_2$AR binds to PDE4D8 and PDE4D9 at the PM (25, 37) but not to PDE4D5 because it is located in the nucleus (38). Agonist stimulation promotes the dynamic association of $\beta_2$AR with different PDE4D isoforms, including transient recruitment of arrestin3-mediated PDE4D3 and PDE4D5 isoforms (39–41). The dynamic binding between $\beta_2$AR and PDE4D isoforms is consistent with the transient recruitment of arrestin to the activated receptor, suggesting that temporary export of PDE4D5 from the nucleus permits cAMP signaling inside the nucleus for gene expression. Inhibition of GRK prevents PDE4D interaction with $\beta_2$AR (27). Our findings demonstrated that mutating the GRK phosphorylation sites blocked ISO-stimulated receptor endocytosis, nuclear export of PDE4D5, nuclear cAMP signal, PKA-mediated IEG expression, and long-term memory in an MWM paradigm, thus confirming the necessity of $\beta_2$AR endocytosis in promoting gene expression (16). Additionally, our observations suggested that some $G\alpha_s$-coupled GPCRs caused the nuclear export of PDE4D5 in cortical neurons.

Moreover, disrupting the arrestin3/PDE4D interaction using a myristoylated peptide (42) blocked the nuclear export of PDE4D5 and cAMP signal in the nucleus without affecting

$\beta_2$AR endocytosis. These data suggest that the endocytosis of GRK-phosphorylated $\beta_2$AR alone is insufficient for the receptor to deliver cAMP signals to the nucleus and that nuclear export of PDE4D5 to the endosome is also required. In this scenario, endosomal cAMP signaling is likely suppressed or restricted locally by PDE4D isoforms that are recruited to GRK-phosphorylated $\beta_2$AR. However, a subset of endosomal $\beta_2$ARs without PDE4D binding may still signal to adenylyl cyclase 9 (43) and promote cAMP production to the nucleus. Therefore, we propose that the recruitment of arrestin and PDE4D5 to GRK-phosphorylated $\beta_2$AR on endosomes functionally sequesters PDE4D5, facilitating cAMP signal propagation from the PM or endosomes to the nucleus. Moreover, a nuclear but not cytosolic PKI inhibits $\beta_2$AR-induced gene expression in hippocampal neurons, supporting the local activation of PKA for gene expression in the nucleus (44). However, our data do not preclude the diffusion of PKA catalytic subunits from the cytoplasm to the nucleus, which could promote gene expression in fibroblasts under specific stimulation (45). Additionally, the local cAMP signals at endosomes may facilitate the activation of ERK and CaMKII pathways by the cAMP-activated guanine-nucleotide exchange factor EPAC (46, 47), resulting in additional cellular actions.

Arrestin-biased agonists such as carvedilol (48) have positive effects on memory consolidation (49), extinction (50), and learning in various disease models (51–53). However, it is yet to be determined whether these effects depend on GRK phosphorylation of $\beta_2$AR. Although the arrestin3/PDE4D complex is critical in the formation of fear memory (54), arrestin3 KO mice display normal memory retention in MWM and EPM performance. The discrepancy between arrestin3 KO and GRKΔ mice highlights our gaps in understanding the exact role of arrestin and GRK phosphorylation in neurons and the need for further research into the underlying mechanisms. These data, however, collectively support the notion that GRK phosphorylation and arrestin3-mediated $\beta_2$AR signaling are necessary for memory consolidation. Although GRKΔ-$\beta_2$AR fails to promote nuclear cAMP signaling, inhibiting PDE4 rescues nuclear signaling and long-term memory deficits in GRKΔ mice. This critical role for PDE4D in $\beta_2$AR-induced nuclear cAMP signaling is further corroborated by evidence indicating that inhibiting this enzyme improves memory in Alzheimer's models (55–58). Additionally, arrestin2 may work together with arrestin3 to regulate $\beta_2$AR and PDE4D isoform localization, thus allowing for fine-tuning of subcellular cAMP signaling in a cell- and tissue-specific manner (32).

We observed that GRKΔ mice had deficits in IEG expression following MWM learning, whereas both WT and mutant mice had strong IEG expression following FST, which tests acute stress responses. These data suggest that IEG expression mediated by acute stress utilizes a different receptor pathway than IEG expression for learning and memory. This is further supported by the finding that $\beta_1$AR-mediated nuclear cAMP signaling remained intact in GRKΔ neurons, consistent with the early finding that $\beta_1$AR is involved in behavioral stress responses (59). $\beta_1$AR and $\beta_3$AR are both involved in memory (60), and $\beta_1$AR resides in various intracellular compartments, including the Golgi, ER/SR, and nuclear envelope (61–65). Thus, the activation of $\beta_1$AR on the nuclear envelope may signal to the nucleus to induce stress responses, even in GRKΔ mice. Despite its weak interaction with arrestins 2 and 3 and its minimal, if any, clathrin-mediated internalization (66–69), $\beta_1$ARs can catalyze the formation of clathrin-coated structures. These structures accumulate

arrestins and release them, allowing downstream signaling to occur (70). Additionally, $\beta_2$AR could work synergistically with other adrenoceptor subtypes by sequestering nuclear PDE4D5 to facilitate the nuclear cAMP accumulation and gene expression.

Together, our data support that a subpopulation of GRK-phosphorylated $\beta_2$AR is necessary to promote the nuclear export and recruitment of PDE4D isoforms, which is critical for facilitating receptor-cAMP signal propagation into the nucleus, IEG expression, and long-term memory in an MWM paradigm. These data highlight a mechanism by which GPCR stimulation can promote the nuclear export of PDEs to promote a dynamic system that permits cAMP propagation into the nucleus.

## Materials and Methods

### Animals

Animals were housed in a UC Davis AAALAC certified vivarium on a 12-hour day/night cycle (7 am to 7 pm), grouped 3–5 mice per cage, and provided free access to food and water. $\beta_1$AR/$\beta_2$AR double knockout (DKO) mice were obtained from Jackson Laboratories (Bar Harbor, ME; #003810) to produce P0-P1 postnatal DKO pups. GRKΔ mice were developed by Cyagen Mouse Services (Santa Clara, CA) using CRISPR/Cas9 technology to remove WT $\beta_2$AR and insert a mutant $\beta_2$AR gene containing S355A and S356A mutations (GRKΔ) into the germline of these mice. Upon receipt, these mice were backcrossed 9 times to obtain a clean C57Bl6/J background. These mice are viable and display normal growth and breeding. However, these mice are more sensitive to sudden stressors, likely because the mutant receptors do not desensitize, thereby amplifying the effects of epinephrine or norepinephrine. Stress indicators (thigmotaxis in the Morris water maze), general activity (open field), and anxiety responses (elevated plus maze) were presented in this manuscript to provide a thorough characterization of these mice. GRKΔ and WT mice (Jackson Laboratories, Bar Harbor, ME; #000664) were used to produce P0-P1 pups and 70–130-day old mice for behavioral and biochemical studies. Animals were grouped without blinding but were randomized during experiments. Groups were spread across multiple cages to minimize cage effects. Male and female animals were used in behavioral experiments. All animals were handled according to approved institutional animal care and use committee (IACUC) protocols (#21993, #20641, and #22371) of the University of California at Davis and in accordance with NIH and ARRIVE guidelines for the use of animals.

### Cell culture

Human embryonic kidney 293 (HEK293) cells were obtained from American Type Culture Collection (ATCC, Manassas, VA). Primary mouse hippocampal neurons were isolated and cultured from early postnatal (P0-P1) wild-type C57Bl6/J (Jackson Laboratories), $\beta_1$AR/$\beta_2$AR double knockout (DKO), and GRKΔ (developed by Cyagen; Santa Clara, CA) mouse pups as previously described (14). Briefly, pups were decapitated, brains were removed and placed in ice-cold HBSS, and hippocampi were dissected out under a dissection scope. Hippocampi were dissociated by 0.25% trypsin treatment in HBSS at 37°C for 16 minutes. After digestion, hippocampi were moved to cold HBSS containing 25% FBS and gently mixed, then into HBSS containing 10% FBS and gently mixed, and finally into HBSS

prewarmed in an incubator containing 5% CO2 at 37°C. Hippocampi were triturated at room temperature using a Pipet-aid (Drummond) set to slow using a 10 mL serological pipet until pieces of tissue were no longer visible. The solution was spun down for 4 minutes at 100 xg and the pellet was resuspended in a Neurobasal medium supplemented with GlutaMax (Thermo Fisher Scientific, Waltham, MA), gentamicin (Promega), B-27 (Thermo Fisher Scientific, Waltham, MA), and 10% FBS. Neurons were plated on poly-D-lysine-coated (Sigma-Aldrich, St. Louis MO: #P6407) #0 12 mm glass coverslips (Glaswarenfabrik Karl Hecht GmbH & Co. KG, Sondheim, Germany; REF 92100100030) for imaging and FRET at a density of 7500 cells/$cm^2$ and 10,000 cells/$cm^2$, respectively.

For cortical gene expression experiments, WT cortical neurons were plated in 6-well polystyrene plates at a density of 100,000 cells/$cm^2$. Neurons were transfected using the $Ca^{2+}$ phosphate method as previously described (14). Briefly, cultured neurons at either 3–5 day in vitro (DIV), 6–8 DIV, or 10–12 DIV were switched to pre-warmed Eagle's minimum essential medium (EMEM, Thermo Scientific, MA) supplemented with GlutaMax 1 hour before transfection. The conditioned media were saved. DNA precipitates were prepared by 2×HBS (pH 6.96 DKO neurons, pH 7.02 WT and GRKΔ neurons) and 2 M $CaCl_2$. After incubation with DNA precipitates for 1 h, neurons were incubated in 10% $CO_2$ pre-equilibrium EMEM for 20 min, which was replaced with the conditioned media. WT and GRKΔ neurons were transfected with PM-ICUE3 using Lipofectamine3000 (Thermo Fisher Scientific, Waltham, MA) following the manufacturer's protocol. FRET biosensors PM-ICUE3 and NLS-ICUE3 have been previously described (71).

**Brain Slicing, Fractionation, Western Blot, and cAMP measurement—**WT and GRKΔ male mice (8–12 weeks) were decapitated and brains placed into ice-cold artificial cerebrospinal fluid (ACSF; in mM: 119 NaCl, 26 $NaHCO_3$, 1.3 $NaH_2PO_4$•$2H_2O$, 3 KCl, 2.5 $CaCl_2$•$2H_2O$, 1.3 $MgSO_4$•7H2O and 11 D-glucose, 305 mOsm/kg, saturated with 95% $O_2$, and 5% $CO_2$; final pH 7.3). About one-third of the rostral and caudal ends of the brain were trimmed off. Per mouse, a total of 4 400-μm-thick forebrain slices containing hippocampus were prepared with a vibratome (Leica VT 1000A). Slices were equilibrated in oxygenated ACSF for 1 h at 32°C before being transferred to incubation chambers and equilibration for 10 min at 32°C in vehicle (ACSF) or clenbuterol (1 μM) solutions. Slices were extracted with hypotonic buffer containing protease and phosphatase inhibitors as above before nuclei were fractionated with 500 g spin for 5 minutes. Nuclear fractions were rinsed and analyzed by Western blot.

Hippocampi excised from the brains of handled control animals were used for this study. Hippocampi were excised, flash-frozen in liquid nitrogen, and stored at −80 °C until use. Tissue was homogenized in lysis buffer (25 mmol/L HEPES, ph 7.4; 5 mmol/L EDTA; 150 mmol/L NaCl; 0.5% Triton X-100; and protease inhibitors containing 2 mmol/L $Na_3VO_4$, 1 mmol/L PMSF, 10 mmol/L NaF, 10 μg/mL aprotinin, 5 mmol/L bestatin, 10 μg/mL leupeptin, and 2 μg/mL pepstatin A). Protein was quantified using a Pierce BSA assay (ThermoFisher, #23225) and read on a CLARIOStar plate reader (BMG Labtech, Cary, NC). Equal amounts of protein (50 μg) were resolved on 8% acrylamide SDS-PAGE gels. Bands were detected using anti-$\beta_2$AR (Santa Cruz #sc-570 lot# L0809), anti-PDE4 (Abcam # ab14628), anti-PDE4D5 (FabGennix # PDE4D5–451AP), anti-PKA IIα (M20, Santa Cruz

#sc-909), and anti-γ-tubulin (Sigma-Aldrich #T7451). Primary antibodies were revealed with IRDye 800 CW goat anti-mouse IgG secondary antibody (1:5000 #926–32210, Licor, NE) or IRDye 800 CW goat anti-rabbit IgG secondary antibody (1:5000 #926–32211, Licor, NE) using a Bio-Rad ChemiDoc MP Imager (Bior-Rad Laboratories, Hercules, CA). The optical density of bands was analyzed using Image J software (NIH; https://imagej.nih.gov/ij/). The arbitrary unit (A.U.) for Western blot signals was defined as the ratio of the intensity of the protein of interest relative to the intensity of a reference protein as indicated.

Hippocampi extracted from WT C57Bl6/J or GRKΔ mice aged 70–130 days were solubilized according to the manufacturer's protocols (Promega cAMP Glo Max, V1681, Madison, WI). cAMP levels were determined from a dilution curve using a microplate reader (CLARIOStarPlus, BMG Labtech).

## Co-Immunoprecipitation assays

Co-immunoprecipitation assays was carried out with HEK293 cells homogenized in 0.4 mL of lysis buffer and centrifuged for 30 minutes at 4°C and 16,100 xg. Supernatants were transferred to fresh centrifuge tubes, and 10 μL Protein A-Sepharose beads (GE17–0780-01, Millipore, MA) and 1.0 μg of control IgG antibody (sc-66931, SCBT, CA) were added. Tubes were incubated for 1 hour at 4C to preclear samples. Precleared samples (1 mL) were incubated with 30 μL Protein A-Sepharose beads and 2 μg of anti-Flag M1 (Sigma-Aldrich, # F3040) or anti-IgG antibody (sc-66931, SCBT, CA) at 4°C overnight. After incubation, beads were rinsed with lysis buffer 3 times. The washed beads were mixed with 30 μL 2x SDS loading buffer (#161–0747, Bio-Rad Laboratories, CA), subjected to electrophoresis, and Western blotted for FLAG-$\beta_2$AR, Nb80, and PDE4D5. Gel images were taken and quantified using a Bio-Rad ChemiDoc MP Imager.

## Fluorescence Resonance Energy Transfer (FRET)

FRET measurements were performed as previously described (25). Briefly, DKO primary hippocampal neurons were co-transfected with FLAG-$\beta_2$AR (WT, GRKΔ, or PKAΔ) and either PM-ICUE3 or NLS-ICUE3 using the calcium phosphate method. WT or GRKΔ primary hippocampal neurons were transfected with NLS-ICUE3 using the calcium phosphate method. Cells were imaged on a Zeiss Axiovert 200M microscope and FRET measurements were performed as previously described. Briefly, DKO primary hippocampal neurons were isolated and plated on poly-D-lysine coated glass cover slips. On DIV 7–10, DKO neurons were co-transfected with FLAG-$\beta_2$AR (WT, GRKΔ, or PKAΔ) and either PM-ICUE3 or NLS-ICUE3 using the calcium phosphate method overnight. WT or GRKΔ primary hippocampal neurons isolated and plated on poly-D-lysine coated glass coverslips were transfected with NLS-ICUE3 using the calcium phosphate method on DIV 3–7 for ~16 hours. Coverslips were placed into 35 mm recording dishes with glass bottoms (D35–20-0-N, Cellvis, Mountain View, CA) containing PBS without calcium. Cells were imaged on a Zeiss Axiovert 200M microscope with a 40×/1.3 numerical aperture oil immersion lens, DV dual view imaging system (Photometrics, AZ), and a cooled CCD camera using MetaFluor software. Dual emission imaging of CFP and YFP was acquired simultaneously with a 420DF20 excitation filter, a 450DRLP dichroic mirror, and two emission filters

(475DF40 for CFP and 535DF25 for YFP). Acquisition was set to 0.2 s long exposures every 20 s. Images in both channels were subjected to background subtraction before ratios of yellow-to-cyan were calculated at each time point. For FRET traces, ratios were normalized to baseline. Maximum FRET ratios were calculated as % change from baseline after treatment. All inhibitors were added prior to recording and allowed to incubate except for PDE inhibitors, which were added concurrently with ISO to avoid any adaptive changes caused by preincubation.

### qRT-PCR analysis

Total RNA was extracted from cells and tissue following treatment and behavioral protocols using Tri-Reagent (Sigma-Aldrich T9424, St. Louis, MO) according to the manufacturer's protocols. Briefly, cells and tissues were homogenized in Tri-Reagent and phase-separated using chloroform. The clear, aqueous layer was transferred to a fresh tube and precipitated with isopropyl alcohol. Following precipitation, the RNA pellet was washed twice using 80% ethanol, dried, and mixed with RNAse/DNAse-free water. Genomic DNA was removed using a DNAse kit (Sigma-Aldrich AMPD1) per the manufacturer's protocol. RNA was quantified using a CLARIOStarPlus microplate reader. Reverse transcription was carried out on extracted RNA using a high-capacity cDNA reverse transcription kit (Applied Biosystems #4368814) and a thermocycler (Veriti 96-well Thermal Cycler, Applied Biosystems). qRT-PCR analysis was performed on cDNA using PowerUp SYBR Green Master Mix (Applied Biosystems, #A25742) and appropriate primers (table S1) using a QuantStudio3 Real-Time PCR system (Applied Biosystems).

### Confocal Microscopy

WT hippocampal neurons were isolated as described above. At DIV 9, cells were transfected with mEYFP-FLAG-$\beta_2$AR using the calcium phosphate method described above. The next day, cells were pretreated with Arr2 peptide (1 μM), mutated control peptide (1 μM), and barbadin (50 μM) for 30 minutes; CGP20207a (3 μM) for 5 minutes; and with or without isoproterenol (1 μM) for 30 minutes. Cells were rinsed with ice-cold PBS without calcium, fixed with 4% paraformaldehyde for 20 minutes, and rinsed with ice-cold PBS without calcium again. Cells were permeabilized using ice-cold PBS containing 0.2% Triton-X100 and 2% goat serum for 15 minutes and washed three times with ice-cold PBS containing 0.05% Triton-X100, 0.2% BSA, and 0.2% goat serum. Coverslips were dried and mounted on glass slides using anti-fade mounting media containing DAPI (H1500-Vector Laboratories, Burlingame, CA) and left to dry overnight. Confocal imaging was carried out using a Leica Falcon SP8 FLIM microscope using a 63x/1.4 oil objective.

WT and GRKΔ hippocampal neurons were isolated as described above. At DIV 14, cells were treated with or without 1 μM isoproterenol for 30 minutes. Cells were fixed and permeabilized as described above. Coverslips were incubated with PDE4D5 (1:50, Abcam Ab14626, Cambridge, UK) antibody overnight at 4°C. Coverslips were washed and incubated with goat anti-rabbit IgG (H+L) Alexa-488 secondary antibody (1:1000, Invitrogen A-11034, Waltham, MA) in the dark and washed again. Coverslips were mounted on glass slides using anti-fade mounting media containing DAPI (H1500-Vector Laboratories, Burlingame, CA) and imaged as described above.

WT primary cortical neurons were isolated as described above. At DIV 10–14, cells were treated with or without 1 μM of either adenosine, isoproterenol, 1μM adenosine, AngII, cGRP, Dopamine, histamine, isoproterenol, PGE1, PEG2, urocortin, or yohimbine for 30 minutes. Cells were fixed and permeabilized as described above. Coverslips were incubated with PDE4D5 (1:50, Abcam Ab14626, Cambridge, UK) antibody overnight at 4°C. Coverslips were washed and incubated with goat anti-rabbit IgG (H+L) Alexa-488 secondary antibody (1:1000, Invitrogen A-11034, Waltham, MA) in the dark, washed again. Coverslips were mounted on glass slides and imaged as described above.

Primary hippocampal neurons isolated from $\beta_1/\beta_2$AR double knockout (DKO) mice at 7–14 DIV were transfected with cAMP biosensor PM-ICUE3 or NLS-ICUE3 together with FLAG-tagged human $\beta_2$AR as described above. Cells were fixed and permeabilized as described above. Coverslips were dried, mounted on glass slides, and imaged as described above.

Primary hippocampal neurons isolated from $\beta_1/\beta_2$AR double knockout (DKO) mice at 7–14 DIV were transfected with FLAG-tagged human $\beta_2$AR as described above. Cells were fixed and permeabilized as described above and incubated with primary antibody against phosphorylated $\beta_2$AR (pS261/262 - Clone 2G3 and 2E1, or pS355/356 – clone 10A5, kindly provided by Dr. Richard Clark, UT Houston) overnight. Cells were washed, incubated with secondary antibodies for 1 hour at room temperature, and washed again. Coverslips were dried and mounted on glass slides, and imaged as described above.

WT MEF and PDE4D KO MEFs were plated at a density of 20,000 cells per glass coverslip and allowed to grow to 60,000 cells per glass coverslip. Cells were fixed and permeabilized as described above. Coverslips were incubated with PDE4D5 (1:50, Abcam Ab14626, Cambridge, UK) antibody overnight at 4°C. Coverslips were washed, incubated with goat anti-rabbit IgG (H+L) Alexa-488 secondary antibody (1:1000, Invitrogen A-11034, Waltham, MA) in the dark, and washed again. Coverslips were mounted on glass slides and imaged as described above.

Brain tissues were harvested, cryosliced, and mounted as described below. Mounted slices were permeabilized using ice-cold PBS containing 0.2% Triton-X100 and 2% goat serum for 15 minutes and then washed with ice-cold PBS containing 0.05% Triton-X100, 0.2% BSA, and 0.2% goat serum three times. Slices were dried. Coverslips were mounted and imaged as described above.

## Behavioral analyses

Mice were handled for 5 days prior to maze testing to acclimate mice to technicians and were moved prior to the start of behavioral tests (Supplemental Figure S5A). For treatment groups, animals were vehicle gavaged during handling. This handling procedure and movement to the maze room without testing was conducted for handling control groups used for qRT-PCR analysis. Before each day of behavioral testing, mice were moved to the testing room and allowed to acclimate for 1 hour. Sessions were recorded using an overhead camera, and, where indicated, mice were tracked using AnyMaze Software version 4.99b. Heat maps were generated from raw X and Y coordinate output from AnyMaze

and processed using RStudio (RStudio, Waltham, MA). Group sizes were determined from established literature. Treatment groups were pseudorandomly distributed within animal cages to minimize cage effects. For behavior tasks except working memory Morris water maze and the FST, 2–3 age matched cohorts were used.

The Morris water maze (MWM) was used to assess spatial learning in memory in rodents. Using distal cues surrounding the maze, animals learned to locate a submerged, invisible escape platform. Spatial learning was assessed across repeated trials over several days. Reference (long-term memory of the learned task) was assessed in a probe trial by removing the platform and allowing the rodent to freely swim and monitoring their performance with tracking software (72, 73). The maze consisted of a water tank 110 cm in diameter and a clear escape platform approximately 10 cm in diameter. Cues (white on black background) were placed at the four cardinal points of the maze wall. Water was clouded using non-toxic tempera paint, kept at 2 cm above the submerged escape platform, and maintained at 25 ± 2°C. Mice were placed in the maze at a start point in front of one of the maze cues on the perimeter facing the maze wall. Animals were allowed to swim until they found the platform or 60 seconds had elapsed. Animals that did not find the escape platform in the time allotted were guided to the platform, where they remained for 10 seconds. If the animal left before 10 seconds had elapsed, they were returned to the platform and gently held there for 10 seconds. The acquisition phase of the maze consisted of four spatial learning trials that took place over 5 days using each of the four start points each day in a pseudorandom order. The probe trial, which assesses memory retention, occurred 24 hours after the last trial. The mice were again placed in the maze between the triangle and plus-sign maze cues in quadrant 3 (Figure 4A) with the platform removed. The animals swam freely for 60 seconds and were tracked by an overhead camera and tracking software. The tracking software defined the thigmotaxis zone as a ring 7 cm in width around the edge of the maze perimeter. A mouse was excluded from analysis if they spent 90% of their time in the start quadrant during the probe trial, which was taken as an indicator of floating. Data points were also excluded if they were detected as an outlier using the ROUT method with Q set to 1% in Prism software (GraphPad Inc., San Diego, CA). Two WT and one GRKΔ mice were excluded using these methods.

Three days prior to maze testing, mice were gavaged using vehicle only (200 μL) to acclimate all groups to the procedure. Mice were weighed the day before water maze testing with PDE4 inhibitor therapy was conducted to determine the dosage of the drug. Roflumilast (Ark Pharm, Inc.; AK110425) was administered at 3 mg/kg. Roflumilast was dissolved in DMSO and added to vehicle to yield a concentration of 0.4 mg/mL roflumilast and 10 μL/mL DMSO to vehicle. Gavage volumes based on animal weight and dosage were rounded to the nearest 50 μL, which allowed for gavage volumes of 200–300 μL. The vehicle consisted of 0.5% carboxymethylcellulose (Sigma-Aldrich #419338) and 2% polysorbate 20 (Acros Organics # 23336–0010) dissolved in Milli-Q water. 10 μL of DMSO per mL of the vehicle was also added to be consistent with roflumilast groups. Roflumilast and vehicle were made fresh just before administration and were kept in the dark and on ice. One hour prior to maze testing, roflumilast or vehicle was administered to the pretreatment and vehicle groups. Three hours after the end of maze testing, the post-treatment group was

administered roflumilast for the duration of maze learning. Animals were not administered drugs or vehicles before the probe trial.

The working memory water maze (WM-MWM) was used to assess working memory in rodents. The procedure used the same maze setup and platform as the standard MWM with the following changes as described previously (72, 73). Each day, the animals were placed in the maze at a single start position and a fixed escape platform location (Figure S6A). Animals performed four 60-second trials each day from this same start position. The following day, they repeated the same training pattern for a new start position and platform location. Mice underwent training for 6 days. Mice were monitored using overhead camera and tracking software. Mice were excluded if they failed to learn the platform location after 6 days of training. One WT and one GRKΔ mouse were excluded using this method. The first two runs on the day of testing were excluded due to platform misplacement. Data are presented as the average of the four daily trials for all six days of learning. For three days of training, platform locations were close to the start location and for the other 3 days of training, platform locations were far from start locations (Figure S6A) to eliminate search pattern and start location-platform location variability effects. Simple linear regression was used to determine the learning.

The forced swim test (FST) is one of the most commonly used behavioral assays for assessing depressive-like behavior in rodents with high interlaboratory reliability (74). It is also an acute stress test (75). It and other acute stress tests induce IEG expression (76). After acclimation, mice were placed into a clear cylindrical tank 200 mm in diameter, and 300 mm tall with water to a depth of 225 mm held at room temperature (25 ± 2 C) with an opaque barrier surrounding 3 sides and were allowed to swim for a total of 6 minutes. The procedure was recorded using overhead camera and scored for active and passive behaviors by a blinded technician.

The elevated plus maze (EPM) Is one of the most widely used assays for assessing anxiety-like behavior in mice and takes advantage of the natural tendency of mice to explore novel environments and their aversion for open and elevated spaces (77). The EPM consisted of open and closed arms arranged in a cross with two open arms and two walled-in, closed arms. The maze was 1050 mm tall. Each arm was 1180 mm long and 110 mm wide. The closed arms had walls 180 mm high. The center intersection of the maze measured 110 mm by 110 mm. Prior to testing, the maze was cleaned with 70% ethanol so that all mice experienced the same scent environment. Mice were placed in the center space facing away from the technician and allowed to freely explore the maze for 5 minutes. Each trial run was recorded, and parameters such as distance traveled, number of arm entries, time spent in each arm, and percent entry into open arm were tabulated using AnyMaze software. After the end of each trial, the mice were put back in their home cages, and the maze apparatus was cleaned with 70% ethanol, removing any waste and scent cues. Mice were excluded if they jumped off the maze apparatus.

The open field activity assay is used to assess general motility and activity. It consisted of an open-top box with plastic sides measuring approximately 355 mm x 355 mm and 455 mm tall. AnyMaze tracking software and an overhead camera tracked the animals' movements

within the chamber. The mouse was placed in the center of the field, facing away from the technician, and allowed to freely explore the field for 10 minutes. Upon completion of the testing trial, the animal was returned to its home cage, and the maze was cleaned with 70% ethanol, removing any waste and scent cues.

### Brain Tissue Harvest

Following completion of maze training or handling, animals were anesthetized with isoflurane, brains removed, and hippocampi excised as previously described. Briefly, tissue was snap-frozen for biochemical analysis, fixed in 10% buffered formalin phosphate (SF100, Thermo Fisher Scientific, Waltham MA) at 4°C for histochemical staining, or placed in TRI reagent (T9424, Sigma-Aldrich, St. Louis, MO) for RNA extraction. After 3 days in formalin, brains were transferred to 30% sucrose and left a minimum of 3 days to dehydrate at 4°C. Following dehydration, brains were mounted in Tissue Tek OCT medium (#4853, Sakura Finetek, Torrance, CA), frozen, and cryo-sectioned using a Leica CM1860 cryostat into 40 μM sections, which were mounted onto tissue-specific glass slides (Thermo-Fisher #12–550-15, Waltham, MA) for staining.

### Cartoon development.

Diagrams were created with BioRender.com.

## Data Analysis

Pooled data were represented as means ± SEM. Fully blinded analysis was performed with different persons carrying out the experiments and analysis, respectively. Representative figures and images reflected the average levels of each experiment. Data were analyzed using GraphPad Prism9 software (GraphPad Inc., San Diego, CA) and expressed as means ± S.E.M. as indicated in figure legends. Normality of the data was assessed using two-sided Kolmogorov–Smirnov test in GraphPad Prism 9. Differences between two groups were assessed by an appropriate two-tailed unpaired Student's *t*-test. Differences among three or more groups were assessed by one-way ANOVA with Tukey's post hoc test. $p < 0.05$ was considered statistically significant. Linearity of learning curves was determined using simple linear regression with statistically non-linear curves determined at $p<0.05$.

## Supplementary Material

Refer to Web version on PubMed Central for supplementary material.

## Acknowledgments:

We would like to thank Dr. Kyle Ireton for use and modification of the R-script used in generating heat maps for this manuscript.

### Funding:

National Institutes of Health Grant GM129376 (YKX), National Institute of Health Grant T32GM099608 (JMM, YKX), National Institute of Health Blueprint Diversity Specialized Predoctoral to Postdoctoral Advancement in Neuroscience Grant F99NS120523 (JMM).

## Data and Materials Availability:

All data needed to evaluate the conclusions in the paper are present in the paper or the Supplementary Materials. The reagents generated for this study are available from Y.K.X. under a material transfer agreement with University of California, Davis, USA.

## References and Notes


1. Lefkowitz RJ, A brief history of G-protein coupled receptors (Nobel Lecture). Angew Chem Int Ed Engl 52, 6366–6378 (2013); published online EpubJun 17 (10.1002/anie.201301924). [PubMed: 23650015]
2. Gao V, Suzuki A, Magistretti PJ, Lengacher S, Pollonini G, Steinman MQ, Alberini CM, Astrocytic beta2-adrenergic receptors mediate hippocampal long-term memory consolidation. Proc Natl Acad Sci U S A 113, 8526–8531 (2016); published online EpubJul 26 (10.1073/pnas.1605063113). [PubMed: 27402767]
3. Levin ED, Petro A, Rezvani AH, Pollard N, Christopher NC, Strauss M, Avery J, Nicholson J, Rose JE, Nicotinic alpha7- or beta2-containing receptor knockout: effects on radial-arm maze learning and long-term nicotine consumption in mice. Behav Brain Res 196, 207–213 (2009); published online EpubJan 23 (10.1016/j.bbr.2008.08.048). [PubMed: 18831991]
4. Branca C, Wisely EV, Hartman LK, Caccamo A, Oddo S, Administration of a selective beta2 adrenergic receptor antagonist exacerbates neuropathology and cognitive deficits in a mouse model of Alzheimer's disease. Neurobiol Aging 35, 2726–2735 (2014); published online EpubDec (10.1016/j.neurobiolaging.2014.06.011). [PubMed: 25034342]
5. Ramos BP, Colgan LA, Nou E, Arnsten AF, Beta2 adrenergic agonist, clenbuterol, enhances working memory performance in aging animals. Neurobiol Aging 29, 1060–1069 (2008); published online EpubJul (10.1016/j.neurobiolaging.2007.02.003). [PubMed: 17363115]
6. Cipres-Flores FJ, Segura-Uribe JJ, Orozco-Suarez S, Guerra-Araiza C, Guevara-Salazar JA, Castillo-Garcia EL, Soriano-Ursua MA, Farfan-Garcia ED, Beta-blockers and salbutamol limited emotional memory disturbance and damage induced by orchiectomy in the rat hippocampus. Life Sci 224, 128–137 (2019); published online EpubMay 1 (10.1016/j.lfs.2019.03.043). [PubMed: 30905783]
7. Ciccarelli M, Sorriento D, Coscioni E, Iaccarino G, Santulli G, in Endocrinology of the Heart in Health and Disease, Schisler JC, Lang CH, Willis MS, Eds. (Academic Press, 2017), pp. 285–315.
8. Yin JC, Tully T, CREB and the formation of long-term memory. Curr Opin Neurobiol 6, 264–268 (1996); published online EpubApr (10.1016/s0959-4388(96)80082-1). [PubMed: 8725970]
9. Kandel ER, The molecular biology of memory: cAMP, PKA, CRE, CREB-1, CREB-2, and CPEB. Mol Brain 5, 14 (2012); published online EpubMay 14 (10.1186/1756-6606-5-14). [PubMed: 22583753]
10. Iyer V, Tran TM, Foster E, Dai W, Clark RB, Knoll BJ, Differential phosphorylation and dephosphorylation of beta2-adrenoceptor sites Ser262 and Ser355,356. Br J Pharmacol 147, 249–259 (2006); published online EpubFeb (10.1038/sj.bjp.0706551). [PubMed: 16331289]
11. Daaka Y, Luttrell LM, Ahn S, Della Rocca GJ, Ferguson SS, Caron MG, Lefkowitz RJ, Essential role for G protein-coupled receptor endocytosis in the activation of mitogen-activated protein kinase. The Journal of biological chemistry 273, 685–688 (1998); published online EpubJan 9 ( [PubMed: 9422717]
12. Daaka Y, Luttrell LM, Lefkowitz RJ, Switching of the coupling of the beta2-adrenergic receptor to different G proteins by protein kinase A. Nature 390, 88–91 (1997); published online EpubNov 6 (10.1038/36362). [PubMed: 9363896]
13. Qian H, Patriarchi T, Price JL, Matt L, Lee B, Nieves-Cintron M, Buonarati OR, Chowdhury D, Nanou E, Nystoriak MA, Catterall WA, Poomvanicha M, Hofmann F, Navedo MF, Hell JW, Phosphorylation of Ser1928 mediates the enhanced activity of the L-type Ca2+ channel Cav1.2 by the beta2-adrenergic receptor in neurons. Sci Signal 10, (2017); published online EpubJan 24 (10.1126/scisignal.aaf9659).

14. Shen A, Nieves-Cintron M, Deng Y, Shi Q, Chowdhury D, Qi J, Hell JW, Navedo MF, Xiang YK, Functionally distinct and selectively phosphorylated GPCR subpopulations co-exist in a single cell. Nature communications 9, 1050 (2018); published online EpubMar 13 (10.1038/s41467-018-03459-7).
15. Vaughan DJ, Millman EE, Godines V, Friedman J, Tran TM, Dai W, Knoll BJ, Clark RB, Moore RH, Role of the G protein-coupled receptor kinase site serine cluster in beta2-adrenergic receptor internalization, desensitization, and beta-arrestin translocation. The Journal of biological chemistry 281, 7684–7692 (2006); published online EpubMar 17 ( [PubMed: 16407241]
16. Tsvetanova NG, von Zastrow M, Spatial encoding of cyclic AMP signaling specificity by GPCR endocytosis. Nature chemical biology 10, 1061–1065 (2014); published online EpubDec (10.1038/nchembio.1665). [PubMed: 25362359]
17. Mittal S, Bjornevik K, Im DS, Flierl A, Dong X, Locascio JJ, Abo KM, Long E, Jin M, Xu B, Xiang YK, Rochet JC, Engeland A, Rizzu P, Heutink P, Bartels T, Selkoe DJ, Caldarone BJ, Glicksman MA, Khurana V, Schule B, Park DS, Riise T, Scherzer CR, beta2-Adrenoreceptor is a regulator of the alpha-synuclein gene driving risk of Parkinson's disease. Science 357, 891–898 (2017); published online EpubSep 1 (10.1126/science.aaf3934). [PubMed: 28860381]
18. Lyga S, Volpe S, Werthmann RC, Gotz K, Sungkaworn T, Lohse MJ, Calebiro D, Persistent cAMP Signaling by Internalized LH Receptors in Ovarian Follicles. Endocrinology 157, 1613–1621 (2016); published online EpubApr (10.1210/en.2015-1945). [PubMed: 26828746]
19. Godbole A, Lyga S, Lohse MJ, Calebiro D, Internalized TSH receptors en route to the TGN induce local Gs-protein signaling and gene transcription. Nature communications 8, 443 (2017); published online EpubSep 5 (10.1038/s41467-017-00357-2).
20. Calebiro D, Nikolaev VO, Gagliani MC, de Filippis T, Dees C, Tacchetti C, Persani L, Lohse MJ, Persistent cAMP-signals triggered by internalized G-protein-coupled receptors. PLoS Biol 7, e1000172 (2009); published online EpubAug (10.1371/journal.pbio.1000172). [PubMed: 19688034]
21. Maity S, Rah S, Sonenberg N, Gkogkas CG, Nguyen PV, Norepinephrine triggers metaplasticity of LTP by increasing translation of specific mRNAs. Learn Mem 22, 499–508 (2015); published online EpubOct (10.1101/lm.039222.115). [PubMed: 26373828]
22. Blackman BE, Horner K, Heidmann J, Wang D, Richter W, Rich TC, Conti M, PDE4D and PDE4B function in distinct subcellular compartments in mouse embryonic fibroblasts. The Journal of biological chemistry 286, 12590–12601 (2011); published online EpubApr 8 (10.1074/jbc.M110.203604). [PubMed: 21288894]
23. Leroy J, Abi-Gerges A, Nikolaev VO, Richter W, Lechene P, Mazet JL, Conti M, Fischmeister R, Vandecasteele G, Spatiotemporal dynamics of beta-adrenergic cAMP signals and L-type Ca2+ channel regulation in adult rat ventricular myocytes: role of phosphodiesterases. Circ Res 102, 1091–1100 (2008); published online EpubMay 9 ( [PubMed: 18369156]
24. Richter W, Day P, Agrawal R, Bruss MD, Granier S, Wang YL, Rasmussen SG, Horner K, Wang P, Lei T, Patterson AJ, Kobilka B, Conti M, Signaling from beta1- and beta2-adrenergic receptors is defined by differential interactions with PDE4. Embo J 27, 384–393 (2008); published online EpubJan 23 ( [PubMed: 18188154]
25. De Arcangelis V, Liu R, Soto D, Xiang Y, Differential association of phosphodiesterase 4D isoforms with beta2-adrenoceptor in cardiac myocytes. The Journal of biological chemistry 284, 33824–33832 (2009); published online EpubDec 4 (10.1074/jbc.M109.020388). [PubMed: 19801680]
26. Perry SJ, Baillie GS, Kohout TA, McPhee I, Magiera MM, Ang KL, Miller WE, McLean AJ, Conti M, Houslay MD, Lefkowitz RJ, Targeting of cyclic AMP degradation to beta 2-adrenergic receptors by beta-arrestins. Science 298, 834–836 (2002); published online EpubOct 25 (10.1126/science.1074683). [PubMed: 12399592]
27. Salazar NC, Vallejos X, Siryk A, Rengo G, Cannavo A, Liccardo D, De Lucia C, Gao E, Leosco D, Koch WJ, Lymperopoulos A, GRK2 blockade with betaARKct is essential for cardiac beta2-adrenergic receptor signaling towards increased contractility. Cell Commun Signal 11, 64 (2013); published online EpubAug 28 (10.1186/1478-811X-11-64). [PubMed: 23984976]

28. Xiang YK, Compartmentalization of beta-adrenergic signals in cardiomyocytes. Circ Res 109, 231–244 (2011); published online EpubJul 8 (10.1161/CIRCRESAHA.110.231340). [PubMed: 21737818]
29. Conti M, Mika D, Richter W, Cyclic AMP compartments and signaling specificity: role of cyclic nucleotide phosphodiesterases. J Gen Physiol 143, 29–38 (2014); published online EpubJan (10.1085/jgp.201311083). [PubMed: 24378905]
30. Xiang Y, Naro F, Zoudilova M, Jin SL, Conti M, Kobilka B, Phosphodiesterase 4D is required for beta2 adrenoceptor subtype-specific signaling in cardiac myocytes. Proc Natl Acad Sci U S A 102, 909–914 (2005); published online EpubJan 18 (10.1073/pnas.0405263102). [PubMed: 15644445]
31. Fischmeister R, Castro LR, Abi-Gerges A, Rochais F, Jurevicius J, Leroy J, Vandecasteele G, Compartmentation of cyclic nucleotide signaling in the heart: the role of cyclic nucleotide phosphodiesterases. Circ Res 99, 816–828 (2006); published online EpubOct 13 (10.1161/01.RES.0000246118.98832.04). [PubMed: 17038651]
32. Zaccolo M, Zerio A, Lobo MJ, Subcellular Organization of the cAMP Signaling Pathway. Pharmacol Rev 73, 278–309 (2021); published online EpubJan (10.1124/pharmrev.120.000086). [PubMed: 33334857]
33. Rasmussen SG, Choi HJ, Fung JJ, Pardon E, Casarosa P, Chae PS, Devree BT, Rosenbaum DM, Thian FS, Kobilka TS, Schnapp A, Konetzki I, Sunahara RK, Gellman SH, Pautsch A, Steyaert J, Weis WI, Kobilka BK, Structure of a nanobody-stabilized active state of the beta(2) adrenoceptor. Nature 469, 175–180 (2011); published online EpubJan 13 (10.1038/nature09648). [PubMed: 21228869]
34. Krasel C, Bunemann M, Lorenz K, Lohse MJ, Beta-arrestin binding to the beta2-adrenergic receptor requires both receptor phosphorylation and receptor activation. The Journal of biological chemistry 280, 9528–9535 (2005); published online EpubMar 11 (10.1074/jbc.M413078200). [PubMed: 15634674]
35. Beautrait A, Paradis JS, Zimmerman B, Giubilaro J, Nikolajev L, Armando S, Kobayashi H, Yamani L, Namkung Y, Heydenreich FM, Khoury E, Audet M, Roux PP, Veprintsev DB, Laporte SA, Bouvier M, A new inhibitor of the beta-arrestin/AP2 endocytic complex reveals interplay between GPCR internalization and signalling. Nature communications 8, 15054 (2017); published online EpubApr 18 (10.1038/ncomms15054).
36. Lobingier BT, von Zastrow M, When trafficking and signaling mix: How subcellular location shapes G protein-coupled receptor activation of heterotrimeric G proteins. Traffic 20, 130–136 (2019); published online EpubFeb (10.1111/tra.12634). [PubMed: 30578610]
37. Li X, Huston E, Lynch MJ, Houslay MD, Baillie GS, Phosphodiesterase-4 influences the PKA phosphorylation status and membrane translocation of G-protein receptor kinase 2 (GRK2) in HEK-293beta2 cells and cardiac myocytes. Biochem J 394, 427–435 (2006); published online EpubMar 1 (10.1042/BJ20051560). [PubMed: 16356165]
38. Clister T, Greenwald EC, Baillie GS, Zhang J, AKAP95 Organizes a Nuclear Microdomain to Control Local cAMP for Regulating Nuclear PKA. Cell Chem Biol 26, 885–891 e884 (2019); published online EpubJun 20 (10.1016/j.chembiol.2019.03.003). [PubMed: 30982750]
39. Shi Q, Li M, Mika D, Fu Q, Kim S, Phan J, Shen A, Vandecasteele G, Xiang YK, Heterologous desensitization of cardiac beta-adrenergic signal via hormone-induced betaAR/arrestin/PDE4 complexes. Cardiovasc Res 113, 656–670 (2017); published online EpubMay 1 (10.1093/cvr/cvx036). [PubMed: 28339772]
40. Zhou XE, He Y, de Waal PW, Gao X, Kang Y, Van Eps N, Yin Y, Pal K, Goswami D, White TA, Barty A, Latorraca NR, Chapman HN, Hubbell WL, Dror RO, Stevens RC, Cherezov V, Gurevich VV, Griffin PR, Ernst OP, Melcher K, Xu HE, Identification of Phosphorylation Codes for Arrestin Recruitment by G Protein-Coupled Receptors. Cell 170, 457–469 e413 (2017); published online EpubJul 27 (10.1016/j.cell.2017.07.002). [PubMed: 28753425]
41. Oakley RH, Laporte SA, Holt JA, Caron MG, Barak LS, Differential affinities of visual arrestin, beta arrestin1, and beta arrestin2 for G protein-coupled receptors delineate two major classes of receptors. The Journal of biological chemistry 275, 17201–17210 (2000); published online EpubJun 2 (10.1074/jbc.M910348199). [PubMed: 10748214]
42. Baillie GS, Adams DR, Bhari N, Houslay TM, Vadrevu S, Meng D, Li X, Dunlop A, Milligan G, Bolger GB, Klussmann E, Houslay MD, Mapping binding sites for the PDE4D5 cAMP-specific

phosphodiesterase to the N- and C-domains of beta-arrestin using spot-immobilized peptide arrays. Biochem J 404, 71–80 (2007); published online EpubMay 15 (10.1042/BJ20070005). [PubMed: 17288540]

43. Lazar AM, Irannejad R, Baldwin TA, Sundaram AB, Gutkind JS, Inoue A, Dessauer CW, Von Zastrow M, G protein-regulated endocytic trafficking of adenylyl cyclase type 9. Elife 9, (2020); published online EpubJun 9 (10.7554/eLife.58039).
44. Sample V, DiPilato LM, Yang JH, Ni Q, Saucerman JJ, Zhang J, Regulation of nuclear PKA revealed by spatiotemporal manipulation of cyclic AMP. Nature chemical biology 8, 375–382 (2012); published online EpubFeb 26 (10.1038/nchembio.799). [PubMed: 22366721]
45. Peng GE, Pessino V, Huang B, von Zastrow M, Spatial decoding of endosomal cAMP signals by a metastable cytoplasmic PKA network. Nature chemical biology 17, 558–566 (2021); published online EpubMay (10.1038/s41589-021-00747-0). [PubMed: 33649598]
46. Miningou Zobon NT, Jedrzejewska-Szmek J, Blackwell KT, Temporal pattern and synergy influence activity of ERK signaling pathways during L-LTP induction. Elife 10, (2021); published online EpubAug 10 (10.7554/eLife.64644).
47. Mika D, Richter W, Conti M, A CaMKII/PDE4D negative feedback regulates cAMP signaling. Proc Natl Acad Sci U S A 112, 2023–2028 (2015); published online EpubFeb 17 (10.1073/pnas.1419992112). [PubMed: 25646485]
48. Lamichhane R, Liu JJ, White KL, Katritch V, Stevens RC, Wuthrich K, Millar DP, Biased Signaling of the G-Protein-Coupled Receptor beta2AR Is Governed by Conformational Exchange Kinetics. Structure 28, 371–377 e373 (2020); published online EpubMar 3 (10.1016/j.str.2020.01.001). [PubMed: 31978323]
49. Liu X, Ma L, Li HH, Huang B, Li YX, Tao YZ, Ma L, beta-Arrestin-biased signaling mediates memory reconsolidation. Proc Natl Acad Sci U S A 112, 4483–4488 (2015); published online EpubApr 7 (10.1073/pnas.1421758112). [PubMed: 25831532]
50. Huang B, Li Y, Cheng D, He G, Liu X, Ma L, beta-Arrestin-biased beta-adrenergic signaling promotes extinction learning of cocaine reward memory. Sci Signal 11, (2018); published online EpubJan 9 (10.1126/scisignal.aam5402).
51. Arrieta-Cruz I, Wang J, Pavlides C, Pasinetti GM, Carvedilol reestablishes long-term potentiation in a mouse model of Alzheimer's disease. J Alzheimers Dis 21, 649–654 (2010)10.3233/JAD-2010-100225). [PubMed: 20571219]
52. Kumar A, Dogra S, Prakash A, Effect of carvedilol on behavioral, mitochondrial dysfunction, and oxidative damage against D-galactose induced senescence in mice. Naunyn Schmiedebergs Arch Pharmacol 380, 431–441 (2009); published online EpubNov (10.1007/s00210-009-0442-8). [PubMed: 19685040]
53. Prakash AK, Kumar A, Effect of chronic treatment of carvedilol on oxidative stress in an intracerebroventricular streptozotocin induced model of dementia in rats. J Pharm Pharmacol 61, 1665–1672 (2009); published online EpubDec (10.1211/jpp/61.12.0012). [PubMed: 19958590]
54. Li Y, Li H, Liu X, Bao G, Tao Y, Wu Z, Xia P, Wu C, Li B, Ma L, Regulation of amygdalar PKA by beta-arrestin-2/phosphodiesterase-4 complex is critical for fear conditioning. Proceedings of the National Academy of Sciences of the United States of America 106, 21918–21923 (2009); published online EpubDec 22 (10.1073/pnas.0906941106). [PubMed: 19955404]
55. Gilleen J, Farah Y, Davison C, Kerins S, Valdearenas L, Uz T, Lahu G, Tsai M, Ogrinc F, Reichenberg A, Williams SC, Mehta MA, Shergill SS, An experimental medicine study of the phosphodiesterase-4 inhibitor, roflumilast, on working memory-related brain activity and episodic memory in schizophrenia patients. Psychopharmacology (Berl) 238, 1279–1289 (2021); published online EpubMay (10.1007/s00213-018-5134-y). [PubMed: 30536081]
56. Vanmierlo T, Creemers P, Akkerman S, van Duinen M, Sambeth A, De Vry J, Uz T, Blokland A, Prickaerts J, The PDE4 inhibitor roflumilast improves memory in rodents at non-emetic doses. Behav Brain Res 303, 26–33 (2016); published online EpubApr 15 (10.1016/j.bbr.2016.01.031). [PubMed: 26794595]
57. Wang H, Zhang FF, Xu Y, Fu HR, Wang XD, Wang L, Chen W, Xu XY, Gao YF, Zhang JG, Zhang HT, The Phosphodiesterase-4 Inhibitor Roflumilast, a Potential Treatment for the Comorbidity of Memory Loss and Depression in Alzheimer's Disease: A Preclinical Study in APP/PS1 Transgenic

Mice. Int J Neuropsychopharmacol 23, 700–711 (2020); published online EpubDec 10 (10.1093/ijnp/pyaa048). [PubMed: 32645141]

58. Ricciarelli R, Brullo C, Prickaerts J, Arancio O, Villa C, Rebosio C, Calcagno E, Balbi M, van Hagen BT, Argyrousi EK, Zhang H, Pronzato MA, Bruno O, Fedele E, Memory-enhancing effects of GEBR-32a, a new PDE4D inhibitor holding promise for the treatment of Alzheimer's disease. Sci Rep 7, 46320 (2017); published online EpubApr 12 (10.1038/srep46320). [PubMed: 28402318]
59. Gorman AL, Dunn AJ, Beta-adrenergic receptors are involved in stress-related behavioral changes. Pharmacol Biochem Behav 45, 1–7 (1993); published online EpubMay (10.1016/0091-3057(93)90078-8). [PubMed: 8100069]
60. Hagena H, Hansen N, Manahan-Vaughan D, beta-Adrenergic Control of Hippocampal Function: Subserving the Choreography of Synaptic Information Storage and Memory. Cereb Cortex 26, 1349–1364 (2016); published online EpubApr (10.1093/cercor/bhv330). [PubMed: 26804338]
61. Irannejad R, Pessino V, Mika D, Huang B, Wedegaertner PB, Conti M, von Zastrow M, Functional selectivity of GPCR-directed drug action through location bias. Nature chemical biology 13, 799–806 (2017); published online EpubJul (10.1038/nchembio.2389). [PubMed: 28553949]
62. Benton KC, Wheeler DS, Kurtoglu B, Bagher Zadeh Ansari M, Cibich DP, Gonzalez DA, Herbst MR, Khursheed S, Knorr RC, Lobner D, Maglasang JG, Rohr KE, Taylor A, Witt PJ, Gasser PJ, Norepinephrine activates β1-adrenergic receptors localized to the inner nuclear membrane in cortical astrocytes. bioRxiv, (2021); published online Epub2021–01-01 00:00:00 (
63. Boivin B, Lavoie C, Vaniotis G, Baragli A, Villeneuve LR, Ethier N, Trieu P, Allen BG, Hebert TE, Functional beta-adrenergic receptor signalling on nuclear membranes in adult rat and mouse ventricular cardiomyocytes. Cardiovasc Res 71, 69–78 (2006); published online EpubJul 1 (10.1016/j.cardiores.2006.03.015). [PubMed: 16631628]
64. Nash CA, Wei W, Irannejad R, Smrcka AV, Golgi localized beta1-adrenergic receptors stimulate Golgi PI4P hydrolysis by PLCepsilon to regulate cardiac hypertrophy. Elife 8, (2019); published online EpubAug 21 (10.7554/eLife.48167).
65. Wang Y, Shi Q, Li M, Zhao M, Reddy Gopireddy R, Teoh JP, Xu B, Zhu C, Ireton KE, Srinivasan S, Chen S, Gasser PJ, Bossuyt J, Hell JW, Bers DM, Xiang YK, Intracellular beta1-Adrenergic Receptors and Organic Cation Transporter 3 Mediate Phospholamban Phosphorylation to Enhance Cardiac Contractility. Circ Res 128, 246–261 (2021); published online EpubJan 22 (10.1161/CIRCRESAHA.120.317452). [PubMed: 33183171]
66. Suzuki T, Nguyen CT, Nantel F, Bonin H, Valiquette M, Frielle T, Bouvier M, Distinct regulation of beta 1- and beta 2-adrenergic receptors in Chinese hamster fibroblasts. Mol Pharmacol 41, 542–548 (1992); published online EpubMar ( [PubMed: 1347641]
67. Shiina T, Kawasaki A, Nagao T, Kurose H, Interaction with beta-arrestin determines the difference in internalization behavor between beta1- and beta2-adrenergic receptors. The Journal of biological chemistry 275, 29082–29090 (2000); published online EpubSep 15 (10.1074/jbc.M909757199). [PubMed: 10862778]
68. Liang W, Curran PK, Hoang Q, Moreland RT, Fishman PH, Differences in endosomal targeting of human (beta)1- and (beta)2-adrenergic receptors following clathrin-mediated endocytosis. J Cell Sci 117, 723–734 (2004); published online EpubFeb 15 (10.1242/jcs.00878). [PubMed: 14734649]
69. Boucrot E, Ferreira AP, Almeida-Souza L, Debard S, Vallis Y, Howard G, Bertot L, Sauvonnet N, McMahon HT, Endophilin marks and controls a clathrin-independent endocytic pathway. Nature 517, 460–465 (2015); published online EpubJan 22 (10.1038/nature14067). [PubMed: 25517094]
70. Eichel K, Jullie D, von Zastrow M, beta-Arrestin drives MAP kinase signalling from clathrin-coated structures after GPCR dissociation. Nat Cell Biol 18, 303–310 (2016); published online EpubMar (10.1038/ncb3307). [PubMed: 26829388]
71. Syed AU, Reddy GR, Ghosh D, Prada MP, Nystoriak MA, Morotti S, Grandi E, Sirish P, Chiamvimonvat N, Hell JW, Santana LF, Xiang YK, Nieves-Cintron M, Navedo MF, Adenylyl cyclase 5-generated cAMP controls cerebral vascular reactivity during diabetic hyperglycemia. J Clin Invest 129, 3140–3152 (2019); published online EpubJun 4 (10.1172/JCI124705). [PubMed: 31162142]

72. Vorhees CV, Williams MT, Morris water maze: procedures for assessing spatial and related forms of learning and memory. Nat Protoc 1, 848–858 (2006)10.1038/nprot.2006.116). [PubMed: 17406317]

73. Vorhees CV, Williams MT, Assessing spatial learning and memory in rodents. ILAR J 55, 310–332 (2014)10.1093/ilar/ilu013). [PubMed: 25225309]

74. Can A, Dao DT, Arad M, Terrillion CE, Piantadosi SC, Gould TD, The mouse forced swim test. J Vis Exp, e3638 (2012); published online EpubJan 29 (10.3791/3638). [PubMed: 22314943]

75. Commons KG, Cholanians AB, Babb JA, Ehlinger DG, The Rodent Forced Swim Test Measures Stress-Coping Strategy, Not Depression-like Behavior. ACS Chem Neurosci 8, 955–960 (2017); published online EpubMay 17 (10.1021/acschemneuro.7b00042). [PubMed: 28287253]

76. Choi SH, Chung S, Cho JH, Cho YH, Kim JW, Kim JM, Kim HJ, Kim HJ, Shin KH, Changes in c-Fos Expression in the Forced Swimming Test: Common and Distinct Modulation in Rat Brain by Desipramine and Citalopram. Korean J Physiol Pharmacol 17, 321–329 (2013); published online EpubAug (10.4196/kjpp.2013.17.4.321). [PubMed: 23946692]

77. Komada M, Takao K, Miyakawa T, Elevated plus maze for mice. J Vis Exp, (2008); published online EpubDec 22 (10.3791/1088).

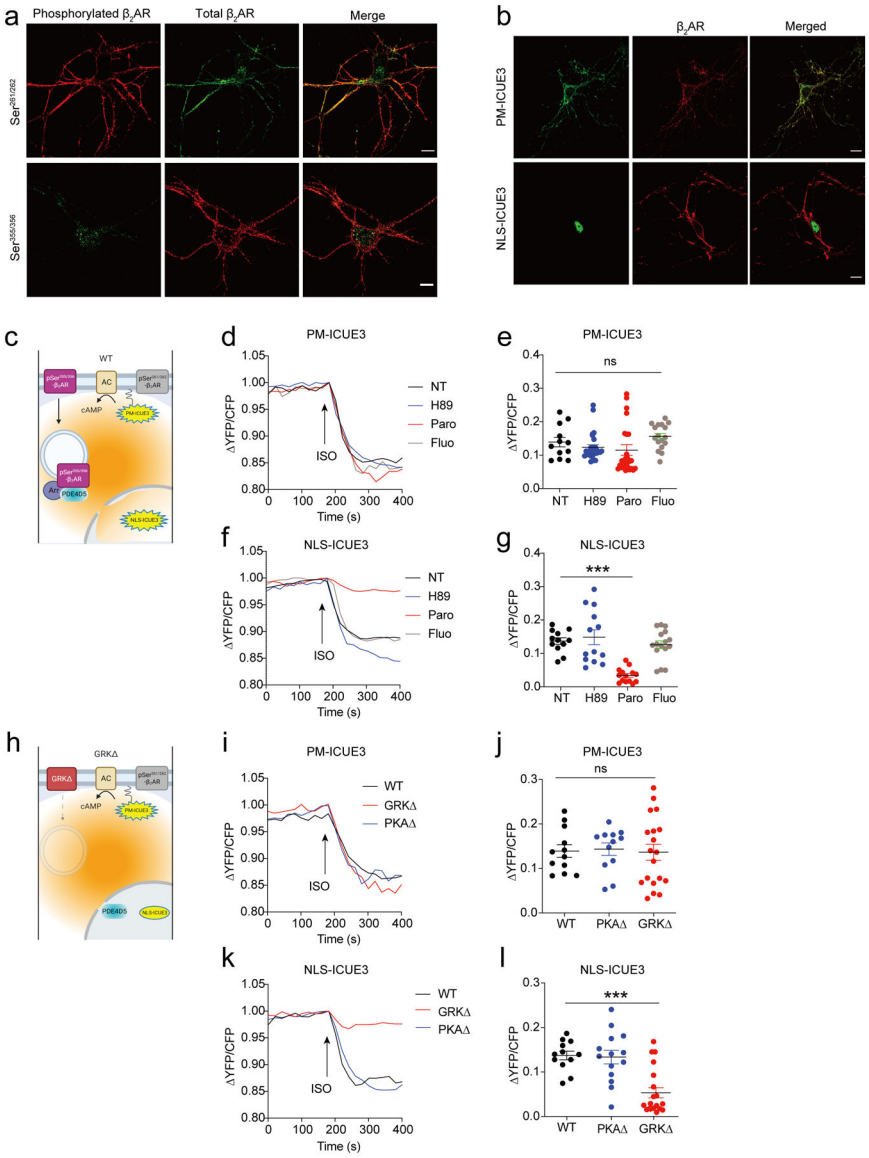


**Fig. 1. Inhibition of GRK or removal of the $\beta_2$AR GRK-phosphorylation sites reduces nuclear cAMP production**

(a) Primary $\beta_1/\beta_2$AR DKO hippocampal neurons were transfected with FLAG-tagged WT-$\beta_2$AR, treated with 1 μM ISO for 5 minutes, and immunostained with antibodies specific for $\beta_2$AR phosphorylated at Ser$^{261/262}$ (by PKA) or Ser$^{355/356}$ (by GRK). Scale bar, 20 μm. (b) Representative images of primary $\beta_1/\beta_2$AR DKO hippocampal neurons transfected with the cAMP biosensor ICUE3 localized to the plasma membrane (PM) or tagged to the nucleus (green) and FLAG-tagged human $\beta_2$AR (red). N = 9–20 cells from five independent experiments. Scale bar, 20 μm. (c) Diagram of subcellular cAMP localization in $\beta_1/\beta_2$AR DKO neurons expressing WT-$\beta_2$AR and ICUE3 biosensors. (d-g) Primary $\beta_1/\beta_2$AR DKO hippocampal neurons were transfected with the cAMP biosensor PM-ICUE3 or NLS-ICUE3 and WT or mutant $\beta_2$AR. Cells were pretreated with H89 (10 μM), paroxetine (Paro, 30 μM), or fluoxetine (Fluo, 30 μM) for 30 minutes before being stimulated with 1 μM ISO. Changes in cAMP FRET ratio were measured. The maximum changes in ICUE3 FRET

(YFP/CFP) ratio relative to baseline after ISO treatment are plotted. Data represent the means ± SEM of individual N = 11–18 neurons from eight isolations per group. ***p<0.001 compared to no-pretreatment (NT) by 1-way ANOVA followed by Tukey's test. (h) Diagram of subcellular cAMP localization in $\beta_1/\beta_2$AR DKO neurons expressing GRKΔ-$\beta_2$AR and ICUE3 biosensors. (i-j) Primary $\beta_1/\beta_2$AR DKO hippocampal neurons were transfected with the cAMP biosensor PM-ICUE3 or NLS-ICUE3 and WT or mutant $\beta_2$AR (S261/262A, PKAΔ, and S355/356A, GRKΔ). Cells were treated with 1 μM ISO and changes in ICUE3 FRET(YFP/CFP) ratio were measured. The maximum changes in ICUE3 FRET ratio induced by ISO are plotted. Data represent the means ± SEM of individual neurons from 8 isolations per group. ***p<0.001 compared WT by 1-way ANOVA followed by Tukey's test.

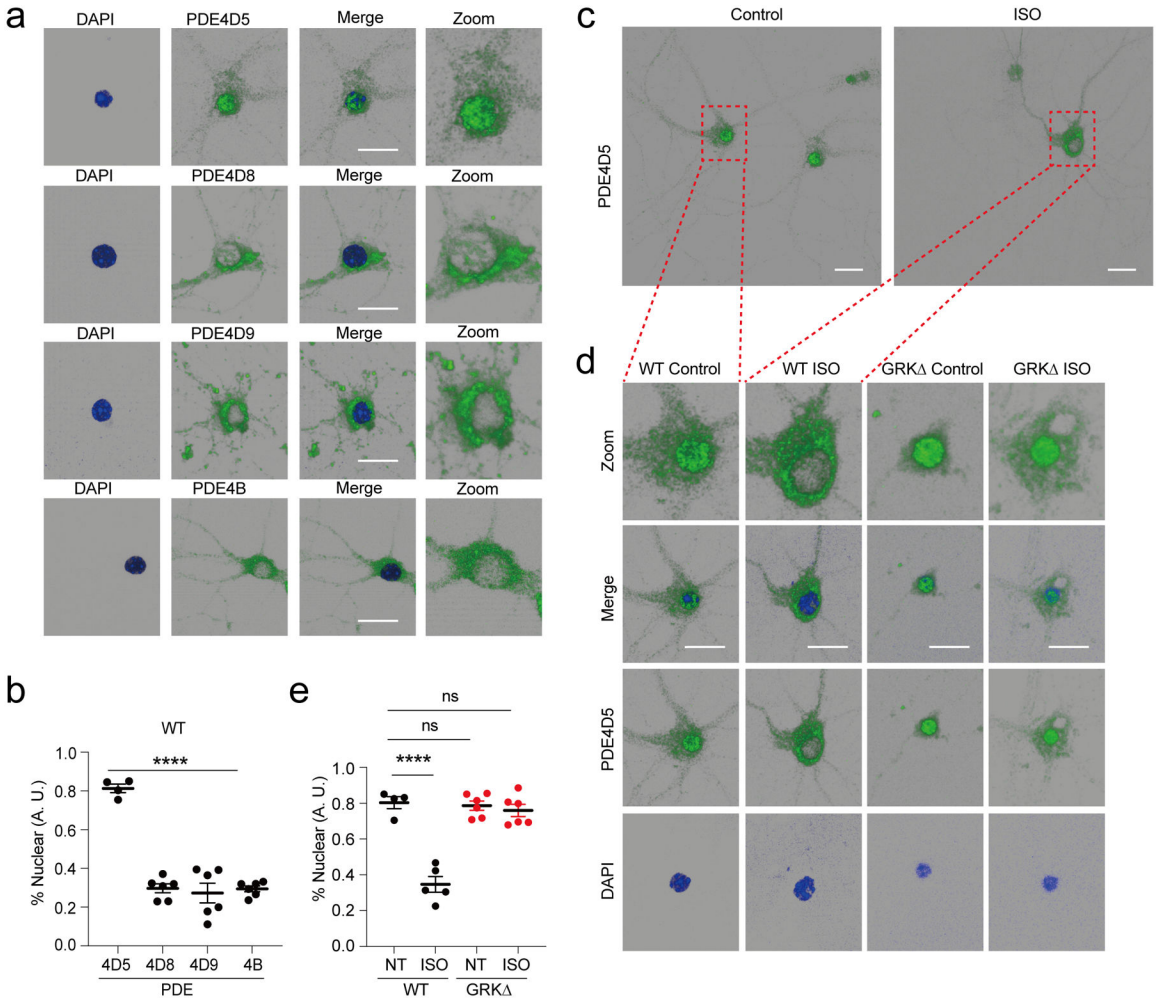


**Fig. 2. GRK-phosphorylated $\beta_2$AR is necessary for agonist induced PDE4D5 trafficking out of the nucleus in neurons.**

(a) Immunofluorescence images of WT primary hippocampal neurons grown to DIV 10–14 and stained for PDE4 isoforms. PDE, Green; DAPI, Blue. Scale bar, 20 μm. (b) Quantification of nuclear PDE4D5 in immunofluorescent images. Data are presented as means ± SEM of individual neurons from 3 independent isolations per group. ****p<0.0001 compared to WT 4D5 by 1-way ANOVA followed by Tukey's test. (c and d) Immunofluorescence images of WT and GRKΔ primary hippocampal neurons at DIV 10–14 with and without ISO stimulation (1 μM, 30 mins). PDE4D5, Green; DAPI, Blue. Scale bar 20 μm in (c) and 20 μm in (d). (e) Quantification of nuclear PDE4D5 in immunofluorescent images. Data are presented as means ± SEM of individual neurons from 3 independent isolations per group. ****p<0.0001 compared WT NT by 1-way ANOVA followed by Tukey's test.

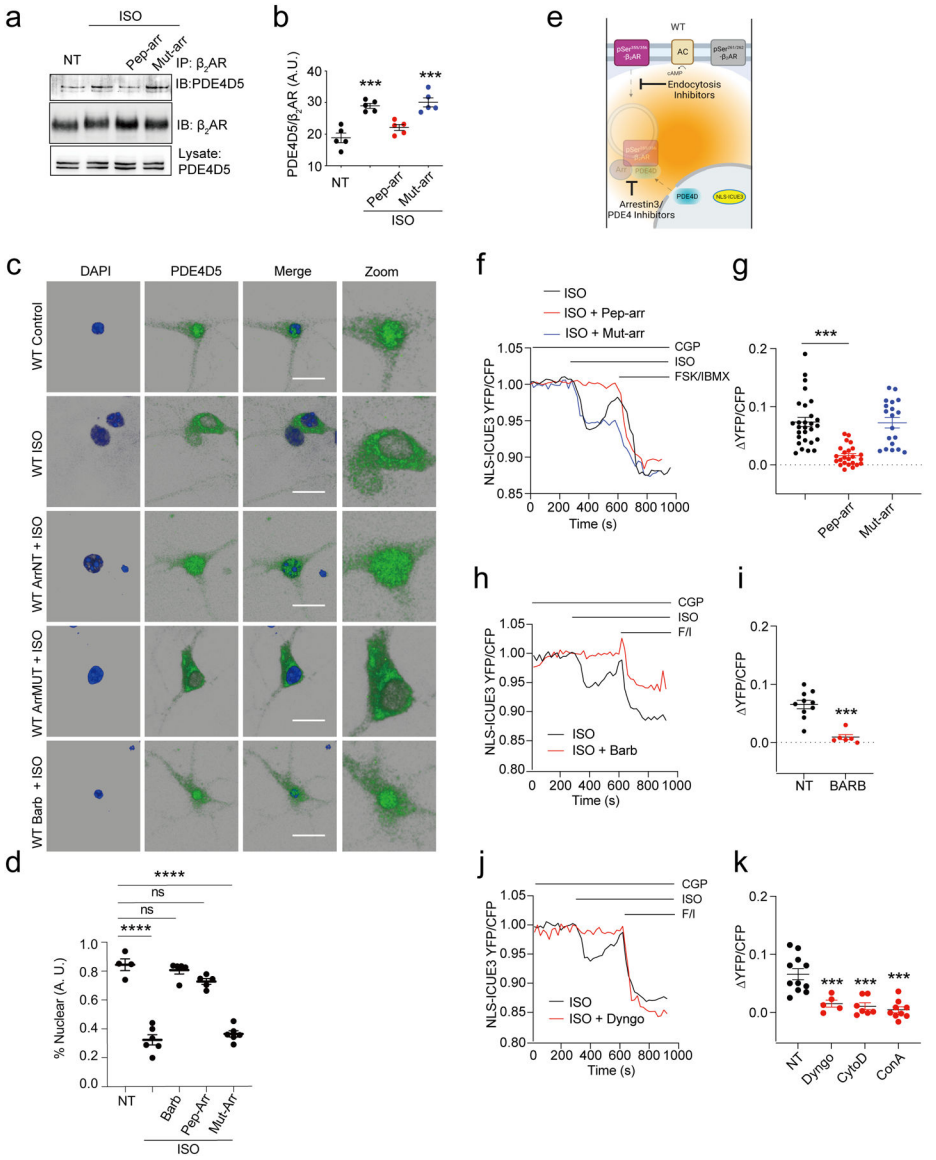


**Fig. 3. The $\beta_2$AR-induced nuclear cAMP signal requires receptor internalization and arrestin/PDE4D5 interaction that facilitates PDE4D5 exclusion from the nucleus.**

(a, b) HEK293 cells transfected with WT-$\beta_2$AR were pretreated with Pep-arr peptide (1 μM, 30 minutes) that disrupts arrestin3-PDE4 binding or control mutant-arr (Mut-arr) peptide before being stimulated with ISO (10 μM, 30 minutes). $\beta_2$AR immunoprecipitates (IP) were immunoblotted (IB) for PDE4D5. Data represent the means ± SEM from 5 individual experiments. ***p<0.001 compared to NT by 1-way ANOVA followed by Tukey's test. (c) Primary WT and GRKΔ hippocampal neurons at DIV 10–14 were pretreated with Pep-Arr peptide (1 μM, 10 mins), mutant control peptide (1 μM, 10 mins), or barbadin (Barb) 50 μM, 30 mins) before being stimulated with 1 μM ISO for 30 mins. Cells were stained with antibodies for PDE4D5 (green) or DAPI (blue). Scale bar = 20 μM (d) Quantification of nuclear/total PDE4D5 in primary hippocampal neurons. Data are presented as means ± SEM of individual neurons from 3 isolations per group. ****p<0.0001 compared to WT NT by 1-way ANOVA followed by Tukey's test. (e) Diagram of FRET experiments. (f, g)

WT primary hippocampal neurons transfected with the cAMP biosensor NLS-ICUE3 were pretreated with Pep-arr or mut-arr peptide (1 μM, 10 minutes) and CGP20712a (300 nM, 5 minutes) before baseline recordings were taken. Neurons were stimulated with ISO (100 nM, 5 minutes), then 10 μM forskolin (FSK) and 1 μM IBMX. Representative traces show changes in the FRET ratio in neurons. Dot plots show the maximum changes in FRET ratio relative to baseline after ISO treatment. Data represent means ± SEM, N = 19–28 neurons from 5 isolations per group. ***p<0.001 compared to NT by 1-way ANOVA followed by Tukey's test. (h, i) Primary WT hippocampal neurons were pretreated with barbadin (50 μM, 30 minutes) before being stimulated with 100 nM ISO, then 10 μM forskolin (FSK) and 1 μM IBMX. The changes in the NLS-ICUE3 YFP/CFP FRET ratio were recorded. Dot plots show the maximum changes in FRET ratio relative to baseline in WT neurons after ISO treatment. Data represent the means ± SEM of individual neurons from 4 isolations per group. ****p<0.001 compared NT by student's t-test. (j, k) Primary WT hippocampal neurons were transfected with the cAMP biosensor NLS-ICUE3. Neurons were treated with 300 nM CGP20217a (CGP), Dyngo4a (Dyngo, 1 μM, 30 minutes), concanavalin A (ConA, 25 ug/ml, 30 minutes), or cytochalasin D (CytoD, 10 μM, 30 minutes) before being stimulated with 100 nM ISO, then 10 μM forskolin (FSK) and 1 μM IBMX. The changes in the ICUE3 YFP/CFP FRET ratio were recorded. Dot plots show the maximum changes in FRET ratio relative to baseline in WT and GRKΔ neurons after ISO treatment. Data represent the means ± SEM of individual neurons from 4 isolations. ***p<0.001 compared to NT by 1-way ANOVA followed by Tukey's test.

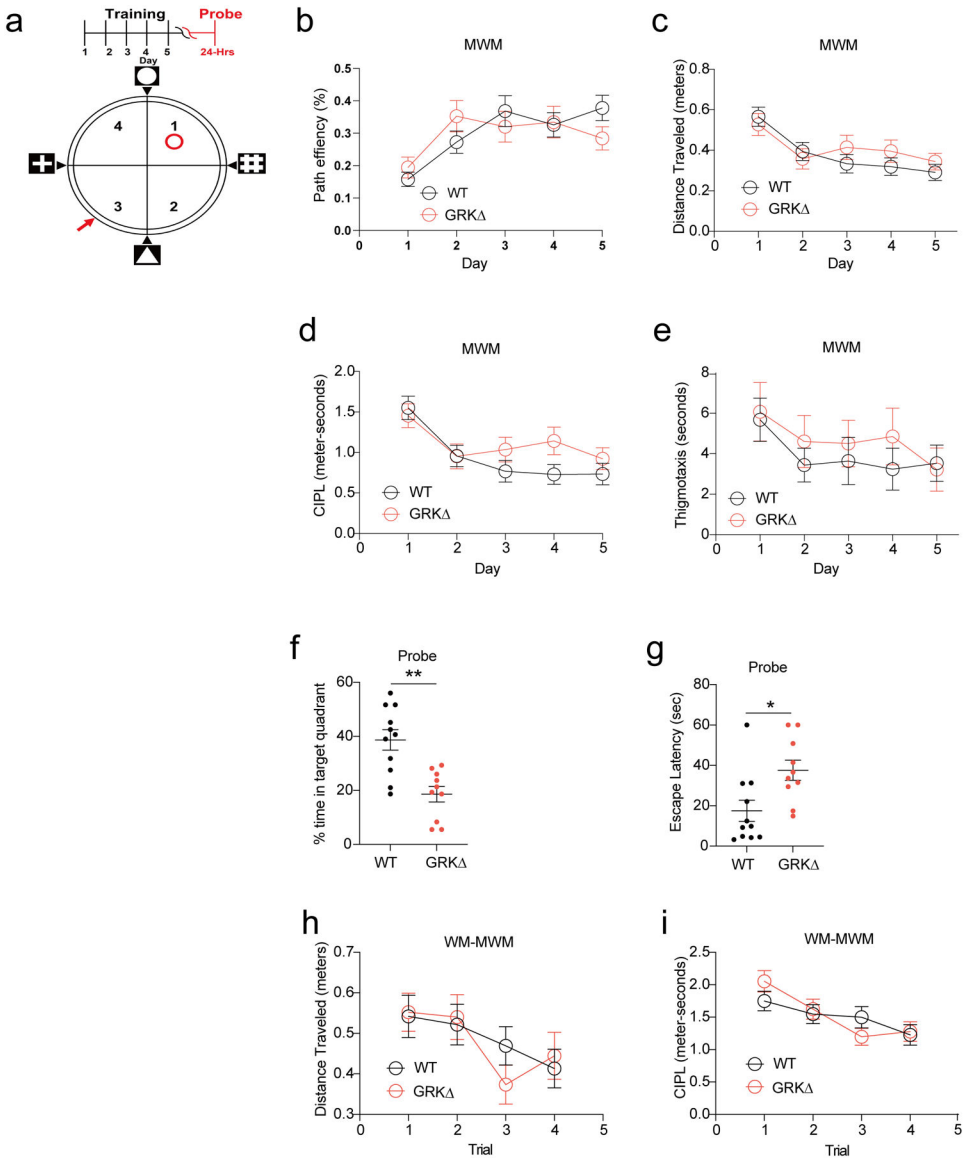


**Fig. 4. Transgenic mice lacking the GRK phosphorylation sites in $\beta_2$AR display defective memory consolidation in a Morris water maze paradigm.**

(a) Diagram of Morris water maze (MWM) testing paradigm. The red arrow indicates the probe start point. Black arrows indicate pseudorandomized training start points. (b) Path efficiency to escape platform. Number of days of training had a significant effect ($p<0.0001$) but group or interaction of day and group did not have an effect, according to 2-way repeated ANOVA analysis between two groups. (c) Distance swum to the escape platform during maze training. Number of days of training had a significant effect ($p<0.0001$) but group or interaction of day and group did not have an effect, according to 2-way ANOVA analysis between two groups. (d) Corrected integrated path length (CIPL), an index of the efficiency of the path taken by the animal to get from starting position to the escape platform normalized for the swim speed to the escape platform. A value of 0 indicates a straight line from start to finish and indicates optimal performance. Number of days of training had a significant effect (****$p<0.0001$) but group or interaction of day and group did not have

an effect, according to 2-way ANOVA analysis between two groups. (e) Thigmotaxis (or proportion of time spent close to maze walls) during testing. Number of days of training, group, or interaction of day and group did not have a significant effect, according to 2-way ANOVA analysis between two groups. (f) Percent time spent in the target quadrant, quadrant 1, during the probe trial. (g) Escape latency (time to first platform entry during the probe trial. Data represent the means ± SEM of individual mice. *$p<0.05$ and **$p<0.01$ by student's t-test. N = 11 WT mice and N = 10 GRKΔ mice for all behavioral metrics b-g. (h, i) Performance metrics (distance traveled and CIPL) between WT and GRKΔ mice in the WM-MWM across 4 daily trials. Number of trials had a significant effect ($p<0.05$ for distance traveled between group and $p<0.001$ for CIPL) but group or interaction of trials and group did not have an effect, according to 2-way ANOVA analysis. Learning curves are significantly non-linear according to linear regression analysis ($p<0.05$). Data represent the means ± SEM of individual mice. N = 5 WT and GRKΔ mice in WM-MWM. *$p<0.05$ and **$p<0.01$ by student's t-test.

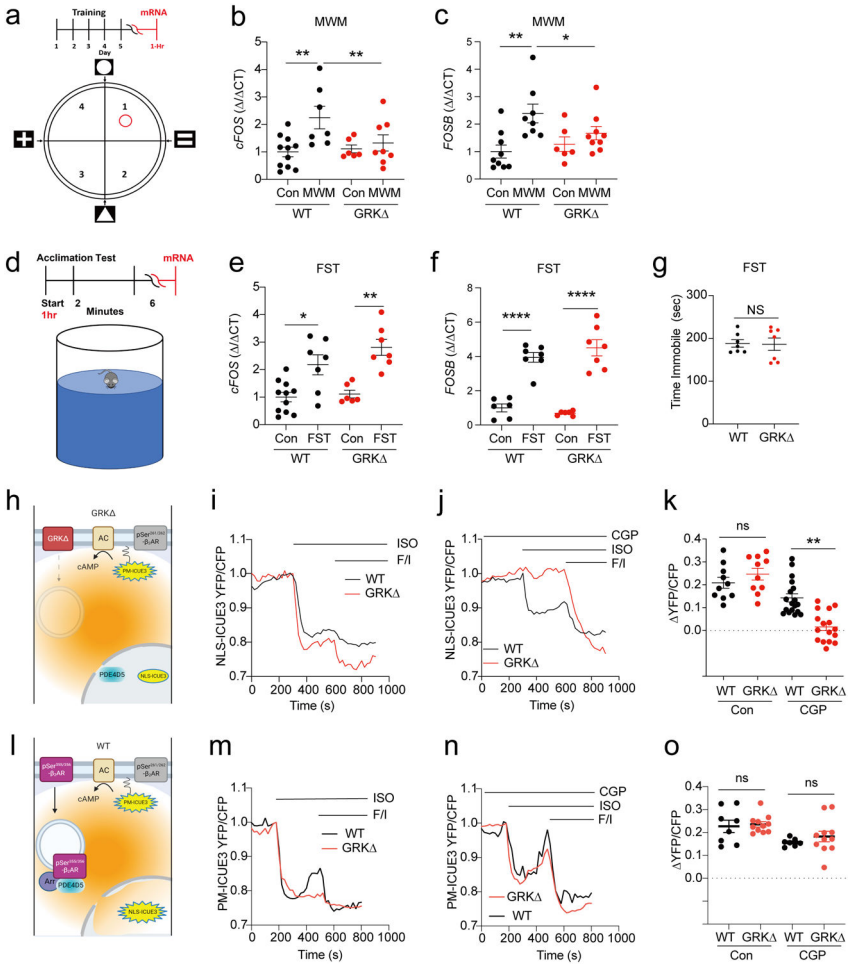


**Fig. 5. Transgenic mice expressing $\beta_2$AR lacking the GRK phosphorylation sites show impaired learning-induced IEG expression.**

(a-c) Transcriptional changes relative to WT control were assessed by qRT-PCR analysis of hippocampi from mice trained on the MWM. Data represent the means ± SEM of individual mice. *cFOS*: n=11 WT mice for control (Con); n=7 WT mice for MWM; n=6 GRKΔ mice for Con; n=8 GRKΔ mice for MWM. *FOSB*: n=9 WT mice for Con; n=8 WT mice for MWM; n=6 GRKΔ mice for Con; n=9 GRKΔ mice for MWM. *p<0.05, **p<0.01 compared to control by 1-way ANOVA followed by Tukey's test. (d) Diagram of FST procedure and RNA isolation from hippocampi at 1 hour after FST exposure. (e, f) Transcriptional changes relative to WT control (con) were assessed by qRT-PCR analysis. (g) Time spent immobile in the FST. Control groups reflect animals that were handled and moved to the maze room in the same manner as tested animals but were not exposed to behavioral paradigms. Data represent the means ± SEM of individual mice. *cFOS*: n=11 WT mice for Con; n=7 WT-mice for FST; n=6 GRKΔ mice for Con; n=7 GRKΔ for FST. *FOSB*: n=6 WT mice for Con; n=7 WT mice for FST; n=6 GRKΔ mice for Con; n=7 GRKΔ mice for FST. *p<0.05, **p<0.01, ****p<0.0001 compared to control by 1-way ANOVA followed by Tukey's test. (h - o) Primary WT or GRKΔ hippocampal neurons were transfected with the cAMP biosensor NLS-ICUE3 or PM-ICUE3. Neurons were pretreated with 300 nM CGP20712a (CGP, 5 minutes) before being stimulated with 100 nM ISO, then

with 10 μM forskolin (FSK) and 1 μM IBMX. The changes in YFP/CFP FRET ratio were recorded. Dot plots show the maximum FRET response (YFP/CFP) ratio relative to baseline in WT and GRKΔ-KI neurons after ISO treatment. Data represent the mean ± SEM, N = 7 −17 neurons isolated from 4 mice per group. ** $p<0.01$ compared to WT by Student's t-test.

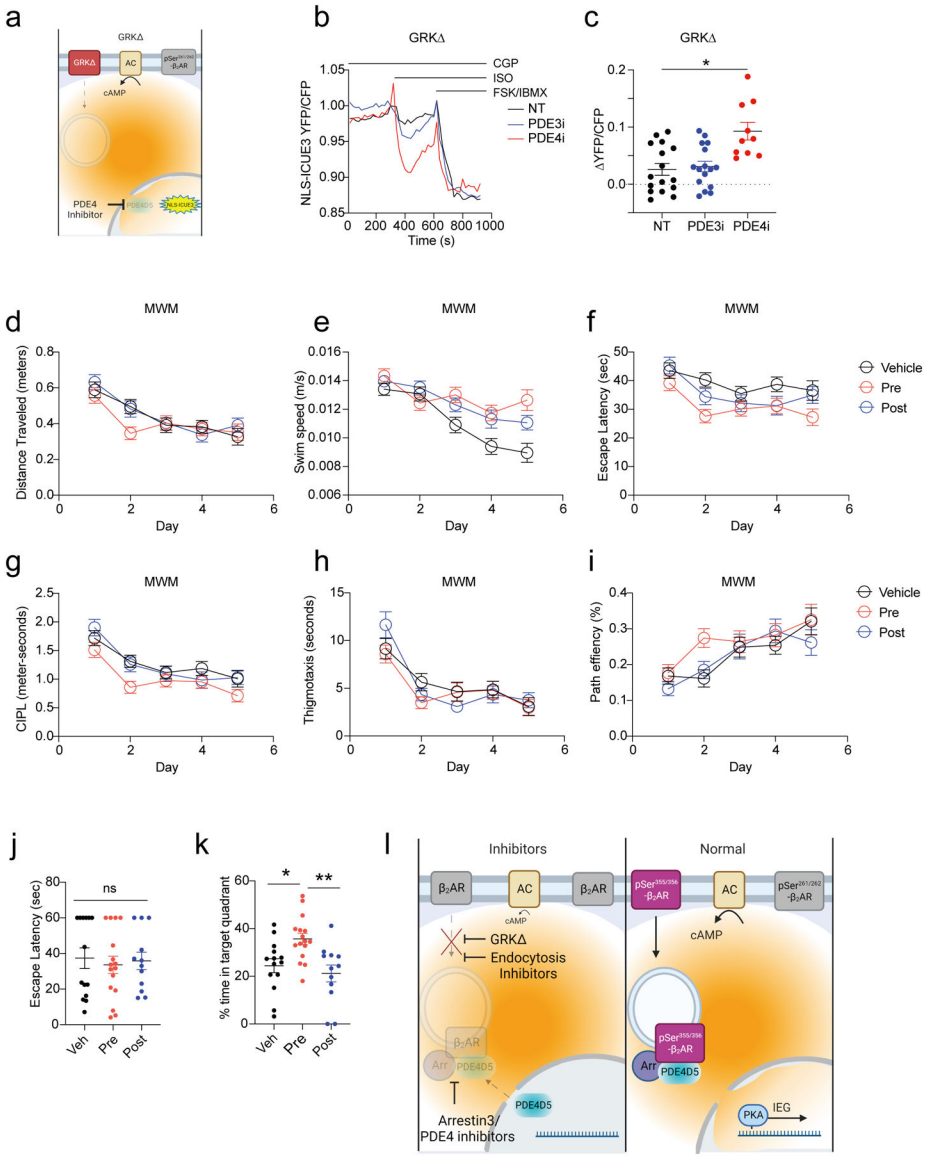


**Fig. 6. Inhibiting PDE4 partially recovers memory retention in the Morris water maze in transgenic mice expressing $\beta_2$AR lacking the GRK phosphorylation sites.**

(a) Diagram of FRET experiments. (b,c) Primary GRKΔ hippocampal neurons transfected with the cAMP biosensor NLS-ICUE3 were stimulated with 100 nM ISO and 100 nM cilostamide (PDE3i) or 100 nM rolipram (PDE4i), then with 10 μM forskolin (FSK) and 1 μM IBMX. Representative traces show changes in the FRET ratio in GRKΔ neurons. Dot plots show the maximum changes in the NLS-ICUE3 FRET ratio relative to the baseline in GRKΔ neurons after ISO treatment. Data represent the mean ± SEM, N = 10 −16 neurons from 4 isolations per group. *p<0.05 compared to NT by 1-way ANOVA followed by Tukey's test. (d – i) Distance traveled (d), swim speed (e), escape latency (f), CIPL (g), thigmotaxis (h), and path efficiency (i) in the MWM performance of GRKΔ mice treated with vehicle (N = 14 mice) or the PDE4 inhibitor roflumilast (3 mg/kg). Mice were treated with roflumilast 1 hour prior to the start of maze testing (pre, n=16 mice) or 3 hours after the completion of maze testing (post, n=12 mice). Number of days of training had a significant

effect ($p<0.0001$) but group or interaction by day and group did not have a significant effect, according to 2-way ANOVA analysis of distance traveled, thigmotaxis, or pathway efficiency among groups. Number of days of training ($p<0.0001$) and group ($p<0.001$) had significant effects but interaction between day and group did not have a significant effect, according to 2-way ANOVA analysis of escape latency among groups. Number of days of training ($p<0.0001$) and group ($p<0.01$) had significant effects but interaction by day and group did not have a significant effect, according to 2-way ANOVA analysis of CIPL among groups. Number of days of training ($p<0.0001$), group ($p<0.001$) and the interaction between day and group ($p<0.01$) had significant effects, according to 2-way ANOVA analysis of swim speed among groups. (j) Escape latency for the probe trial. (k) Percentage of time in target quadrant following maze learning during the probe trial. Data in (j) and (k) represent the means ± SEM of individual mice. *$p<0.05$, **$p<0.01$ compared pretreatment group by 1-way ANOVA followed by Tukey's test. (l) Stimulation of $\beta_2$AR promotes GRK and PKA-mediated phosphorylation of the receptor. The GRK-phosphorylated $\beta_2$AR complex undergoes endocytosis, which subsequently sequesters PDE4D isoforms on endosomes, facilitating the ability of the cAMP signal to reach the nucleus and promote IEG expression.